ARTICLE

Initial, transient, and specific interaction between G protein-coupled receptor and target G protein in parallel signal processing: a case of olfactory discrimination of cancer-induced odors

Takaaki Sato[1], Mutsumi Matsukawa[2], Yoichi Mizutani[3], Toshio Iijima[4], Hiroyoshi Matsumura[5]

Authors' affiliations:

[1] Biomedical Research Institute, National Institute of Advanced Industrial Science and Technology, Osaka, Japan

[2] Division of Anatomical Science, Department of Functional Morphology, Nihon University School of Medicine, Tokyo, Japan

[3] Department of Medical Engineering, Faculty of Health Science, Aino University, Osaka, Japan

[4] Graduate School of Life Sciences, Tohoku University, Sendai, Japan

[5] College of Life Sciences, Ritsumeikan University, Kusatsu, Japan

* **Corresponding author:** Takaaki Sato, Biomedical Research Institute, National Institute of Advanced Industrial Science and Technology, 1-8-31 Midorioka, Ikeda, Osaka 563-8577, Japan, E-mail: taka-sato@aist.go.jp

Abstract:

G protein-coupled receptors (GPCRs) detect and distinguish between various subtypes of extracellular signals, such as neurotransmitters, hormones, light, and odorous chemicals. As determinants for robust and appropriate cellular responses, common and unique features of interactions between GPCRs and their target G proteins provide insights into structure-based drug design for treatment of GPCR-related diseases. Recently, we found that the hydrophobic core buried between GPCR helix 8 and TM1–2 is essential for activation of both specific and nonspecific G proteins. Furthermore, the 2nd residue of helix 8 is responsible for initial, transient, and specific interaction with a target G protein. Analysis of human and murine olfactory receptors (ORs) and other class-A GPCRs revealed that several amino acids, such as Glu, Gln, and Asp, are conserved at this position. This analysis enabled one sub-classification for 64 of 88 non-olfactory GPCR groups associated with a set of agonists and target G protein subtypes, suggesting distinct, subclass-specific functional roles in parallel GPCR signaling pathways. In contrast, class I and II ORs were grouped into two and three sub-classifications, respectively, for one subtype of G_{olf}. In parallel OR signal processing, the response rapidity of helix-8-2nd-Glu ORs via activation of G_{olf} suggests their key role during odor coding. Additionally, sniffer mice discriminated between 0.3 nL urine mixture odors of pre- and post-transurethral resection in individual patients with bladder cancer in an equal-occult blood diluted condition. Future analysis of urine mixtures may provide more robust biomarkers of bladder cancer than those of single individual urine samples.

Keywords: GPCR, drug target, olfaction, adrenergic receptor, rhodopsin, opioid receptor, CX3CR1, bladder cancer, biomarker.

Introduction

In humans, nearly 800 G protein-coupled receptors (GPCRs) [1] distinguish and transduce various extracellular signals and their subtypes from inside the body or from external environments, such as neurotransmitters, hormones, light, and odorous chemicals during neurological, cardiovascular, sensory and reproductive signaling processes. The variability of GPCR signaling systems makes them major therapeutic targets [2]. In addition to classical GPCR activation, five novel modes of GPCR activation, that is, biased activation (arrestin-mediated signaling), intracellular activation, dimerization activation, transactivation, and biphasic activation, were recently reviewed [3]. An analysis of 68,496 individuals revealed that GPCRs targeted by drugs show genetic variation within functional regions such as drug- and effector-binding sites of GPCRs: 8 missense and 0.002 loss-of-function variations per individual as well as two duplications and three deletions per GPCR drug target as copy number variations in the exome aggregation consortium dataset [4].

Despite the diversity of GPCR and G protein signaling pathways, a given subtype of signal specifically activates a subset of GPCRs and leads to robust and appropriate cellular responses via activation of target G proteins. Additionally, in each signaling system, a single to dozens of subtypes of extracellular signals activate in parallel more than one subtype of GPCRs expressed in a single to dozens of subtypes of cells, the resulting signals are also processed in parallel through the signaling pathways (parallel signal processing). Common and unique features of interactions between GPCRs and their target G proteins will provide insights into how the various sets of receptors and G proteins work to distinguish between distinct stimulants and will inform structure-based drug design for the treatment of GPCR-related diseases [4–8]. Based on the principle that the conservation of every residue in a protein with its paralogues and their corresponding orthologues, a comparison of each of the 16 human G protein subtypes with their respective orthologues from 66 genomes revealed the 25 highly conserved, subtype-specifically conserved and neutrally evolving positions of G proteins (Gα selectivity barcode) [5]. In contrast, the receptor selectivity determinants are more complex and dynamic in evolutionary history. In aminergic, vasopressin 2 receptor (V2R)-related, sphingosine-1-phosphate (S1P)-related, and purinergic receptors, distinct signatures of GPCRs in the interface positions (intercellular loop 2, transmembrane domain 3 (TM3), TM5–7 and helix 8) among the subset of closely related receptors that can bind a given Gα family compared with those in the same group that cannot [5]. However, activation processes were not considered.

Recently, by using chimeric G protein and GPCR functional expression system with sub-second time resolution, we found that the hydrophobic core buried between murine olfactory receptor S6 (*m*OR-S6) helix 8 and TM1–2 is essential for activation of both specific and nonspecific G proteins (G_{15_olf}, DDBJ #LC017737 and G_{15}) (Fig. 1, a homology model based on an active-state β_2 adrenergic receptor (β_2AdR)) [6, 7]. In addition, the 2nd residue of helix 8 is re-

sponsible for initial transient and specific interaction with a target G protein, and therefore controls the GPCR response rapidity and subsequent parallel signal processing [6, 7]. Another live cell assay of GPCR and chimeric G proteins also revealed different cellular responses via different subtypes of chimeric G proteins and the same GPCR at 1-minute intervals [8]. In a previous review, various functional roles of amphipathic helix 8 in GPCRs were summarized [6]. In the present review, we compare the 2nd residue of helix 8 in an extended range of non-olfactory GPCRs, and first propose a GPCR activation step model, and its functional role in odor coding as an example of complicated GPCR signal processing. Analysis of the amino acid sequences of hundreds of human and murine ORs and other class-A GPCRs revealed that several amino acids, such as Glu, Gln, and Asp, are conserved at the 2nd position of helix 8 [6]. The conserved residues enable one sub-classification of non-olfactory GPCRs and two of class-I ORs for one subtype of G protein, suggesting distinct, subclass-specific functional roles in parallel GPCR signaling pathways.

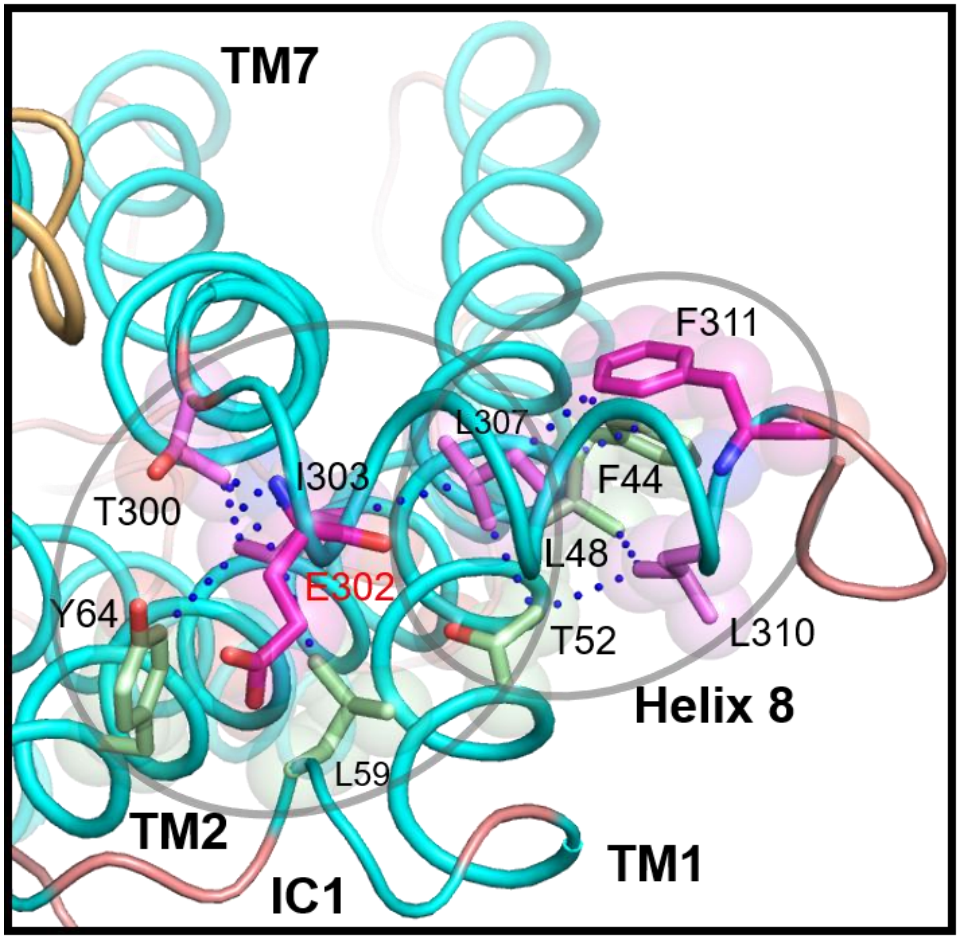

Figure 1. Cytoplasmic view of N-terminal acidic 2nd residue of *m*OR-S6 (GPCR) helix 8 and hydrophobic core (within gray circles) buried between TM1–2 and helix 8 for initial, transient, and specific interaction with G_{olf} (modified from reference [6])

ORs comprise the largest GPCR superfamily, suggesting a great diversity of odorous chemicals as well as their odors. Well-trained police dogs exhibit an amazing ability to distinguish between target and non-target body odors from footprints. Similarly, "sniffer mice," which are trained with an olfactory cue, are able to distinguish between genetically determined mouse urine odors in a Y-maze, even though the mice have large diet-related variations in urine odors [9, 10]. Furthermore, sniffer dogs and mice sensitively distinguish between urine odors of other mice with or without experimental tumors [11] as well as human cancer [12–15]. It is likely that OR genes have evolved such diversity to distinguish between similar but slightly different and important olfactory cues from similar odorous chemicals and their mixtures, such as genetically determined individual body odors and their disease-induced disorders. The number of functional OR genes in mice (ca. 1100) is 1.4-fold that in dogs (ca. 800) and 2.8-fold that in humans (ca. 400) [16], while approximately 70% of human ORs have homologous (orthologous) murine ORs. These facts suggest common principles of receptor coding for odors in mice and humans [17–19], while some similar odors that mice can distinguish between are indiscriminable to dogs and humans.

In olfaction, signals from more than 400 types of ORs are transferred to the olfactory cortex via OR-specific pathways [20, 21]. This means that there are more than 400 parallel OR signaling pathways in the olfactory system [22]. As an emphasizing system for elemental, stimulus-specific information, a hierarchy of elemental odors has been observed in olfactory processing via feedforward inhibition [6, 15, 18, 23, 24]. In addition, after genetic ablation of all dorsal ORs (defined as ORs expressed in the dorsal region of the sensory organ in the manner of one neuron−one receptor) [25, 26], ΔD mice cannot recognize the important odor of their predator [27] and exhibit an odor discrimination paradox, by which they detect (−)-enantiomers with no marked change in detection sensitivity yet display more than 10^{10}-fold reductions in (−)- and (+)-enantiomeric odor discrimination sensitivity [23]. Moreover, the most sensitive dorsal OR to (*R*)-(−)-carvone, a helix-8-2nd-Glu OR, is deleted in ΔD mice, indicating its possible association with an impaired representation or emphasis on the (*R*)-(−)-carvone-unique elemental odor [23]. The response rapidity of helix-8-2nd-Glu ORs via activation of G_{olf} suggests the key role of these receptors in odor representation by weighted combinatorial receptor coding (weighted signal integration) for elemental odors [6, 23]. Thus, helix 8-based subclasses of GPCRs likely play distinct functional roles in parallel GPCR signaling pathways [6].

1. Rapid transition from initial, transient, and specific interactions to shared, stable interactions both in GPCRs and between GPCRs and target G proteins

GPCRs consist of seven transmembrane-spanning α-helices TM connected by extracellular loops (EC) or intracellular loops (IC, including a C-terminal short α-helix, helix 8). When ligands or target G proteins can freely access to GPCR binding sites, a specific interaction with a higher

binding affinity is formed earlier than are shared interactions with relatively lower binding affinities [6]. This specific binding of an agonist or target G protein to its GPCR initiates subsequent conformational changes in the GPCR or GPCR−G protein complex that lead to activation as follows (modified from reference 6) [6].

(1) Semi-activation of GPCR: an agonist molecule binds to a specific binding site on a target GPCR.

(2) Activation of GPCR: binding of a specific agonist induces structural rearrangement of intra-molecular interactions in the GPCR TM domains.

(3) Semi-activation of G protein:

3-1) The activated GPCR initially, transiently, and specifically interacts with a target heterotrimeric G protein.

3-2) When the above, specific interaction does not take place, the activated GPCR occasionally and non-specifically interacts with non-target G proteins.

(4) Full or partial activation of G protein;

4-1) In the initial, transient, and specific interaction between the activated GPCR and a semi-activated target G protein, displacement of helix-α5 of the Gα subunit towards TM3 of the GPCR facilitates the formation of a more stable, ternary, activated GPCR−heterotrimeric G-protein complex mediated by shared and/or partially specific interactions (extensive interaction) [28].

4-2) In the initial, non-specific interaction between the activated GPCR and a semi-activated non-target G protein, a partial interaction is likely to form, causing a partial activation of the G protein.

(5) GDP release from G protein: in the stable, ternary, activated GPCR− heterotrimeric G-protein complex, the Gα subunit releases GDP from the binding pocket.

(6) GTP binding to G protein: a GTP then binds to the nucleotide-free Gα subunit, followed by dissociation of the Gα and βγ subunits from the GPCR.

(7) Activation of effector proteins: the Gα and βγ subunits interact with their respective effector proteins for regulating the effector activities.

As described above, steps (1) and (3) are likely to be specific to a target GPCR or G protein, whereas steps (2) and (4) are likely to be shared between different GPCRs or G proteins [6]. Some GPCR-shared, intra-molecular interactions in step (2) are listed in Table 1 [29–31]. It is possible that the interaction between Tyr7.53 and Phe/Ile8.50 is weakened in step (2) and completely broken in step (4).

Table 1. Shared intra-interaction of GPCRs in inactive → active states (modified from reference [6])

	Extracellular signals	Hormones	Light/Colors	Morphine (Opioid)	
TM domains	GPCR subtypes	β_2 Adrenergic R (G_s)	Rhodopsin/Opsin (G_t)	μOpioid R (G_i)	ref.
TM3, 5	Arg3.50−none→Tyr5.58	Arg^{131}−none→Tyr^{219}	Arg^{135}−Glu^{247} →Tyr^{223}	Arg^{165}−Thr^{279}→Tyr^{252}	29
TM7, helix 8, TM3, 5	Tyr7.53−Phe8.50 →Tyr5.58+Leu3.43	Tyr^{326}−Phe^{332} →Tyr^{219}+Leu^{124}	Tyr^{306}−Phe^{313} →Tyr^{223}+Leu^{128}	Tyr^{336}–Phe^{343} →Tyr^{252}+Leu^{158}	29
TM7,helix 8	Cys7.54−Arg8.51→none	Cys^{327}−Arg^{333}→none	Ile^{307}−Arg^{314}→none	Ala^{337}−Lys^{344}→none	29
TM3, 6, 7	Ile3.46−Leu6.37→Tyr7.53	Ile^{127}−Leu^{275}→Tyr^{326}	Leu^{131}−Val^{254}→Tyr^{306}	Met^{161}−Val^{282}→Tyr^{336}	30

TM, transmembrane domain; R, receptor; x.yz is the Ballesteros-Weinstein numbering method for GPCRs [31].

During steps (1)–(4), activation delays of GPCRs and G proteins are dependent on agonist affinity and GPCR−G protein interaction specificity, respectively. In steps (3) and (4), the structural stability of C-terminal amphipathic helix 8 through the hydrophobic core between helix 8 and TM1–2 plays a critical role in the rapid formation of a stable interaction between a GPCR and its target G protein (Figs. 1, 2, S1) [6, 7]. Helix 8 begins after a short linker following TM7, at the end of which the conserved NPxxY motif is located [32]. In crystal structures of β_2AdR and rhodopsin, helix 8 lies parallel to the membrane in both the inactive and active states [28, 32–34]. Moreover, in the inactive states of these GPCRs, the third residue (Phe) of helix 8 interacts with the Tyr residue of the NPxxY motif in TM7 [28, 33], and mutation within this motif causes a significant reduction in signaling activity [33, 34].

In our homology model (Fig. 1), the hydrophobic core of both the N-terminal linker (Thr^{300}) and helix 8 (Ile^{303}, Leu^{307}, Val^{308}, Leu^{310}, and Phe^{311}) of *m*OR-S6 are surrounded by TM1 (Phe^{44}, Leu^{48}, and Thr^{52}), IC1 (Leu^{59}), and TM2 (Tyr^{64}) [6, 7]. The hydrophobic residues of helix 8 can be categorized into two groups [6, 7]. The first group contains Thr^{300}, Ile^{303}, and Leu^{307}, which are located at the N-terminal region and the middle region of helix 8. These residues and especially the hydrophobic interactions between Ile^{303} and Thr^{300} play crucial roles in appropriately positioning helix 8, and mutation of these residues likely disrupts the hydrophobic core and prevents activation of Gα. The second group of *m*OR-S6 helix 8 hydrophobic residues includes Leu^{310} and Phe^{311}, located at the C-terminal interface between helix 8 and TM1. Our alanine-scanning mutagenesis analysis of helix 8 revealed that the effect of mutating the N-terminus (T300A, I303A) is greater than that of mutating the middle region (L307A) or the C-terminus (L310A, F311A) [7]. Notably, in C-X3-C motif chemokine receptor 1 (CX3CR1), a significant association between human neurodevelopmental disorders (schizophrenia and autism spectrum disorders) and Thr^{52}-corresponding genetic variant CX3CR1-A55T was found, suggesting CX3CR1 signaling impairment by the destabilized hydrophobic core at the middle region or TM1 C-terminus [35] (Suppl. Fig. S2).

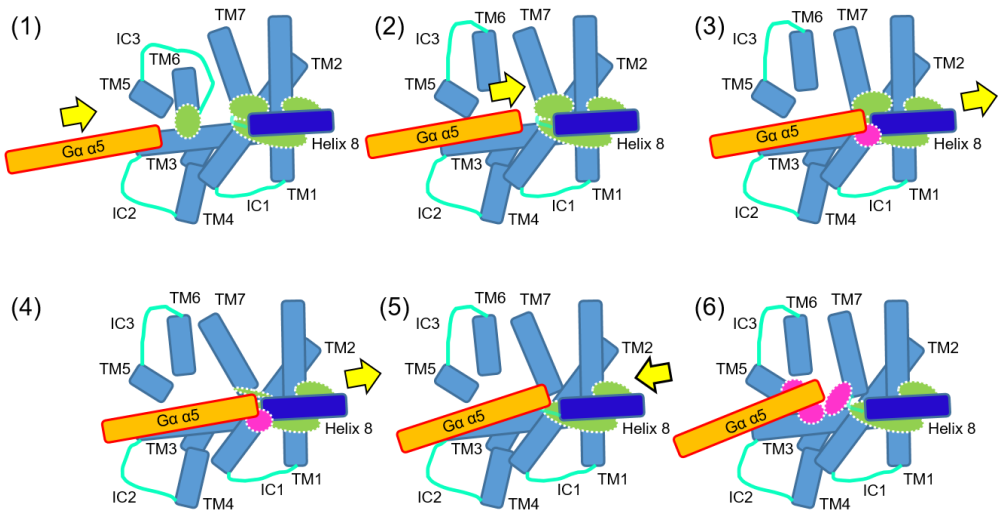

Figure 2. A transition model of multistep interactions between GPCR and its target G protein. (1) Relative movement of the Gα α5 C-terminus toward GPCR helix-8 N-terminus). (2) Trigger of outward movement of TM6 until docking onto the C- and N-termini. (3) Initial, transient, and specific interactions of the Gα α5 C-terminal 6th residue(+) and GPCR helix-8 2nd residue(−) (G_s/G_{olf}–β_2AdR/OR: Arg^{389}/Lys^{369}–Asp$^{8.49}$/Glu$^{8.49}$, marked by the magenta closed circle). (4) Inertial movement of helix 8 breaks the interaction of helix-8–NPxxY (helix8 adjacent Phe$^{8.50}$/Ile$^{8.51}$–Tyr$^{7.53}$, the left one of the green closed circles). (5) Push back of the Gα α5 C-terminus toward GPCR TM3 by inter-TM elastic property of TM7. (6) Stable interactions of GPCR TM3-DRY–Gα α5 C-terminal 4th residue + GPCR NPxxY (Arg$^{3.50}$–Tyr$^{391/371}$ + Tyr$^{7.53}$, the magenta closed circles).

A transition model of multistep interactions between a GPCR and its target G protein is shown in Figure 2. This model was constructed by inserting possible transient processes between the inactive state (1) and active state (6) including the transient specific interaction (3). Considering the simplest case of β_2AdR (or *m*OR-S6) and its relative movement toward Gα, the C-terminus of Gα α5 moves forward towards the N-terminal region of β_2AdR helix 8 under TM domain assembly from the intracellular spacing between TM3 and TM5 [6]. This relative movement is likely the trigger for an outward movement of the intracellular portion of TM6 that resides on the front side of the N-terminus of helix 8. Forward movement of the C-terminal region of Gα α5 would then promote its docking onto the N-terminus of β_2AdR (or *m*OR-S6) helix 8, resulting in the formation of an initial, transient, and specific interaction between Arg^{389}, the 6th residue from the C-terminus of $G\alpha_s$ (in helix-α5; Lys^{369} of $G\alpha_{15\_olf}$), and Asp^{331}, the 2nd residue of β_2AdR helix 8 (Glu^{302} in *m*OR-S6), at the corner of helix 8 and the membrane surface [6]. The next step facilitates the breakage of the remaining interaction between the NPxxY motif Tyr7.53^{326} (Tyr7.53^{296} of *m*OR-S6) and Phe8.50^{332} (Ile8.50^{303} of *m*OR-S6), the 3rd residue of helix 8, which is caused by the inertial outward movement of the adjacent Asp^{331} (Glu^{302} of *m*OR-S6) due to the forward momentum of the transiently interacting Gα C-terminus [6]. This presumably results in the reverse movement of helix 8 in the Gα C-terminus being pushed back towards TM3 through inter-TM interactions with either or both of TM7 and TM2, which underpin the elastic properties and the latter hydrophobic core. This likely results in intimate interactions between β_2AdR TM3 DRY-motif Arg^{131} and both Tyr^{391}, the fourth residue from the C-terminus of $G\alpha_s$, and β_2AdR(*m*OR-S6)

NPxxY-motif Tyr^{326}(Tyr^{296}), as well as interactions between TM5 (Leu^{230}(Tyr^{222}), Glu^{225}(Leu^{217}), and Lys^{232}(Arg^{224})) and $G\alpha_s$($G\alpha_{olf}$/$_{olf\text{-}15}$) α5 (Leu^{394}(Leu^{381}/^{374}), Gln^{384}(Gln^{371}/Leu^{364}), and Asp^{381}(Asp^{368}/^{361})), which stabilize the active state of the ternary complex [28] and lead to rapid and robust activation of G proteins.

When the initial, transient, and specific interactions between GPCRs and their target G proteins do not form, activation of the G protein is delayed and incomplete. Slow and partial activation of $G\alpha_{15}$ by *m*OR-S6 is likely mediated by an interaction between *m*OR-S6 helix 8 Lys^{301} and $G\alpha_{15}$ α4/β6 loop Glu^{328} (murine $G\alpha_{15}$ Asp^{328}). This interaction is observed in the M3 muscarinic acetylcholine receptor (M3R, specific to $G_{q/11}$, M3R helix 8 Lys^{548} and G_q α4/β6 loop Asp^{321}) [36] and results in slower response kinetics than does the inter-helix interaction between *m*OR-S6 and $G\alpha_{15\_olf}$ [6].

2. Classification of olfactory receptors and other GPCRs in parallel signaling pathways

One to three residues of Glu, Gln, Asp, Asn, Trp, His, Lys, and Arg are conserved at the 2nd position of class-A GPCR helix 8 for each GPCR−G protein parallel signaling pathway (Tables 2, Suppl. Figs. S3, S4, ST1) [6]. In the Tables 2 and ST1, ORs and 178 GPCRs are classified by agonist category, the 2nd residue of helix 8, and the subtype of their target G proteins (G_s class, including G_{olf}; $G_{q/11}$ class, including G_{15}; $G_{i/o}$ class, including G_t; and $G_{12/13}$ class). Interestingly, this 2nd residue of helix 8 is negatively charged (Glu or Asp) for 21/64 single-residue non-olfactory subclasses, whereas chemokine receptors likely conserve the positively charged residue (Lys or Arg). A predicted hierarchy of GPCR signaling was determined by the helix-8 2nd residues according to the orders of Glu (4, −) > [Gln (4, none), Asp (3, −)] > Asn (3, none) > [Ser (2, none), Thr (2, none)] > Ala (1, none) for G_s, and Lys (5, +) > Arg (6, +) > Asn (3, none) > Ser (2, none) for G_i based on the lengths and charges of the side chains (as indicated in parentheses). A negative charge on the 2nd residue of helix 8 is considered most suitable for G_s similarly to G_{olf} (as described below), whereas a positive charge is predicted to be most suitable to G_i the opposite charges cause opposite changes in cAMP concentrations via specific interactions with G_s and G_i at the reversed charged residues. This model also requires direct evidence in future study.

Table 2. Classification of GPCRs by helix-8 2nd residues and G protein subtypes (modified from reference [6])

GPCRs	Helix-8 Second Residue											Predicted Hierarchy
	all	Glu	Gln	Asp	Asn	Trp	His	Lys	Arg	misc	Identity	
Human class-I ORs (G_{olf})	52 100%	**12** **23%**	36 69%	**0** **0%**	0 0%	0 0%	1 2%	1 2%	0 0%	2 4%	93% 39/42	helix-8-2nd-Glu ORs > helix-8-2nd-Gln ORs
Murine class-I ORs (G_{olf})	123 100%	**29** **24%**	83 67%	**0** **0%**	0 0%	0 0%	0 0%	5 4%	0 0%	6 5%		
Human class-II ORs (G_{olf})	322 100%	**155** **48%**	22 7%	128 40%	1 0%	0 0%	2 2%	6 2%	0 0%	8 2%	90% 204/226	helix-8-2nd-Glu ORs > helix-8-2nd-Gln or Asp ORs
Murine class-II ORs (G_{olf})	979 100%	**409** **42%**	75 8%	467 48%	7 1%	0 0%	1 0%	6 1%	0 0%	14 1%		
Human TAAR ORs (G_s, G_q, G_i)	6 100%	**0** **0%**	0 0%	0 0%	0 0%	**6** **100%**	0 0%	0 0%	0 0%	0 0%	100% 5/5	
Murine TAAR ORs (G_s, G_q, G_i)	15 100%	**0** **0%**	0 0%	0 0%	0 0%	**15** **100%**	0 0%	0 0%	0 0%	0 0%		
Human Total ORs (odor, G_{olf})	374 100%	**167** **45%**	58 16%	128 34%	1 0%	0 0%	3 1%	7 2%	0 0%	10 3%	91% 243/268	helix-8-2nd-Glu ORs > helix-8-2nd-Gln or Asp ORs
Murine Total ORs (odor, G_{olf})	1102 100%	**438** **40%**	158 14%	467 42%	7 1%	0 0%	1 0%	11 1%	0 0%	20 2%		

Table 2. Classification of GPCRs by helix-8 2nd residues and G protein subtypes (modified from reference [6]) (continued)

GPCRs	Helix-8 Second Residue										Predicted Hierarchy or the 2nd residue
	all	Glu	Gln	Asp	Asn	Trp	His	Lys	Arg	misc	
Rhodopsin/ Opsin (light, G_t)	4 100%	0 0%	**4 100%**	0 0%	0 0%	0 0%	0 0%	0 0%	0 0%	0 0%	
$\beta_{1/2/3}$ Adrenergic Rs (hormone, G_s)	3 100%	0 0%	0 0%	**3 100%**	0 0%	0 0%	0 0%	0 0%	0 0%	0 0%	
α_1 Adrenergic R (hormone, $G_{q/11}$)	1 100%	**1 100%**	0 0%	0 0%	0 0%	0 0%	0 0%	0 0%	0 0%	0 0%	
α_2 Adrenergic R (hormone, $G_{i/o}$)	1 100%	0 0%	0 0%	**1 100%**	0 0%	0 0%	0 0%	0 0%	0 0%	0 0%	
Dopamine D1/5 Rs (neurotransmitter, G_s)	2 100%	0 0%	0 0%	**2 100%**	0 0%	0 0%	0 0%	0 0%	0 0%	0 0%	
Dopamine D2/3/4 Rs (neurotransmitter, $G_{i/o}$)	3 100%	**3 100%**	0 0%	0 0%	0 0%	0 0%	0 0%	0 0%	0 0%	0 0%	
Calcitonin CT R* (hormone, G_s)	1 100%	**1 100%**	0 0%	0 0%	0 0%	0 0%	0 0%	0 0%	0 0%	0 0%	
Glucagon GHRH/GIP/GLP-1/GCG Rs* (hormone, G_s)	4 100%	**4 100%**	0 0%	0 0%	0 0%	0 0%	0 0%	0 0%	0 0%	0 0%	
Adenosine $A_{2A/B}$ Rs (neurotransmitter, G_s)	2 100%	1 50%	0 0%	1 50%	0 0%	0 0%	0 0%	0 0%	0 0%	0 0%	A_{2A}(E) > A_{2B}(D) (G_s)
Adenosine $A_{1/3}$ Rs (neurotransmitter, $G_{i/o}$)	2 100%	0 0%	0 0%	0 0%	0 0%	0 0%	0 0%	**2 100%**	0 0%	0 0%	
Serotonin 5-$HT_{4/6/7}$ Rs (neurotransmitter, G_s)	3 100%	0 0%	0 0%	2 67%	0 0%	0 0%	0 0%	0 0%	0 0%	1 17%	5-HT_6(D)/$_7$(D) > 5-HT_4(S) (G_s)
Serotonin 5-$HT_{1A/B/D/E/F/5A}$ Rs (neurotransmitter, $G_{i/o}$)	6 100%	1 17%	0 0%	4 67%	1 17%	0 0%	0 0%	0 0%	0 0%	0 0%	
Serotonin 5-$HT_{2A/B/C}$ Rs (neurotransmitter, $G_{q/11}$)	3 100%	0 0%	0 0%	0 0%	0 0%	0 0%	0 0%	0 0%	0 0%	3 100%	5-HT_{2A}(T)/$_B$(T)/$_C$(I)
Histamine H1 R (neurotransmitter, $G_{q/11}$)	1 100%	0 0%	0 0%	0 0%	**1 100%**	0 0%	0 0%	0 0%	0 0%	0 0%	
Histamine H2 R (neurotransmitter, $G_{q/11}$ > G_s)	1 100%	0 0%	0 0%	**1 100%**	0 0%	0 0%	0 0%	0 0%	0 0%	0 0%	
Histamine H3/4 Rs (neurotransmitter, $G_{i/o}$)	2 100%	0 0%	0 0%	0 0%	0 0%	0 0%	0 0%	0 0%	1 50%	1 50%	H4(R) > H3(S) (G_i)
Melanocortin MC1/2/3/4/5 Rs (hormone, G_s)	5 100%	**5 100%**	0 0%	0 0%	0 0%	0 0%	0 0%	0 0%	0 0%	0 0%	
Vasopressin V2 R (hormone, G_s)	1 100%	0 0%	0 0%	0 0%	0 0%	0 0%	0 0%	0 0%	0 0%	**1 100%**	V2(S)
Vasopressin V1a/b & Oxytocin OXT Rs (hormone, $G_{q/11}$)	3 100%	0 0%	0 0%	0 0%	0 0%	0 0%	**3 100%**	0 0%	0 0%	0 0%	
Somatostatin SSTR3 R (hormone, $G_{i/o}$ > $G_{q/11}$)	1 100%	0 0%	0 0%	0 0%	0 0%	0 0%	0 0%	0 0%	**1 100%**	0 0%	R3(R) > R1(N)/2(N) /R4(N)/5(N) (G_i)
Somatostatin SSTR1/2/4/5 Rs (hormone, $G_{i/o}$)	4 100%	0 0%	0 0%	0 0%	**4 100%**	0 0%	0 0%	0 0%	0 0%	0 0%	
Glycoprotein Hormone FSH R (hormone, G_s, $G_{i/o}$, $G_{q/11}$)	1 100%	0 0%	0 0%	0 0%	**1 100%**	0 0%	0 0%	0 0%	0 0%	0 0%	FSH(N) > LH(T), TSH(A) (G_s)
Glycoprotein Hormone LH/TSH Rs (hormone, G_s > $G_{q/11}$)	2 100%	0 0%	0 0%	0 0%	0 0%	0 0%	0 0%	0 0%	0 0%	2 100%	LH(T), TSH(A)
Opioid δ/κ/μOpioid/ORL1 Rs (opioid, $G_{i/o}$)	4 100%	0 0%	0 0%	0 0%	**4 100%**	0 0%	0 0%	0 0%	0 0%	0 0%	
Chemokine(C) XCR1 (chemokine, $G_{i/o}$)	1 100%	0 0%	0 0%	0 0%	0 0%	0 0%	0 0%	**1 100%**	0 0%	0 0%	
Chemokine(CC) CCR1–10 Rs (chemokine, $G_{i/o}$)	10 100%	0 0%	0 0%	0 0%	0 0%	0 0%	0 0%	6 60%	4 40%	0 0%	R2(K)/4–8(K) > R1/3/9/10(R) (G_i)?
Chemokine(CXC) CXCR1–7 Rs (chemokine, $G_{i/o}$)	7 100%	0 0%	0 0%	0 0%	2 29%	0 0%	0 0%	5 71%	0 0%	0 0%	R2–6(K) > R1(N)/7(N) (G_i)
Chemokine(CX3C) CX3CR1 (chemokine, $G_{i/o}$)	1 100%	0 0%	0 0%	0 0%	0 0%	0 0%	0 0%	**1 100%**	0 0%	0 0%	

5-HT, 5-hydroxytryptamine; FSH, follicle-stimulating hormone; LH, luteinizing hormone; TSH, thyroid-stimulating hormone. Calcitonin receptor (CT R*), growth hormone releasing hormone receptor (GHRH R*), gastric inhibitory polypeptide receptor (GIP R*), glucagon-like peptide 1 receptor (GLP-1 R*) and glucagon receptor (GCG R*) belong to the class B family of GPCRs, some of which conserve TM7 V(A/S)(V/I/T)(L/I)Y and helix-8 V8.50 instead of the NPxxY motif and F8.50 [37]. G protein: http://www.guidetopharmacology.org.

Of 88 exemplified non-olfactory GPCR subclasses, 64 conserve a single type of residue for each subtype of target G proteins. This highly conserved identity of helix-8 2nd residue strongly suggests that the 2nd residue of helix 8 plays a critical role in selecting target G protein for distinct functional signaling pathways. When helix-8-2nd residues would be identical and critical determinants of initial transient and specific interactions with target G proteins, cellular response delay and robustness are simply determined by agonist affinities with the GPCRs. In subsequent GPCR signaling processing, the signals from the GPCRs most sensitive to a given stimulant are first recognized to control behaviors or other regulatory systems.

In contrast, ORs conserved three types of residues at the position for a single type of G_{olf} (Table 2). Class-I ORs conserve Glu (23% and 24%) and Gln (69% and 67%) in humans and mice, respectively (Table 2) [6]. Interestingly, Glu and Gln are identical in terms of side-chain size (i.e., they are isosteric). However, although Glu and Asp both have a negative charge, the side chain of Asp is shorter by one carbon atom, and there are no helix-8-2nd-Asp ORs among human or murine class-I ORs that are all dorsal ORs [6]. Helix-8-2nd-Glu ORs, with their more rapid activation of G_{olf} than that of helix-8-2nd-Gln ORs, could play a key role in odor representation by multiple OR signal integration [6]. Only trace amine-associated receptors (TAARs) conserve the Trp residue. These four subclass ORs likely play distinct, subclass-specific roles through different response dynamics controlled by the 2nd residue of helix 8. Moreover, the existence of helix-8-2nd-Lys or His ORs (*h*OR56B4 and *h*OR52E6) suggests a possible inhibitory response via G_i in some odor detection.

In order to extract and identify reliable sensory information comprising stimulant-unique and multiple stimulant-common elements with signals from dozens of receptors, logical and stimulant-dependent semi-automatic control is required during parallel and sequential signal processing in the sensory systems. A principal sensory strategy would be one analogous to that in vision. In color vision, the four elemental colors (red, green, yellow, and blue) are primarily extracted by third-order neurons (ganglion cells) or the higher visual pathway through summation of synchronized inputs from one or two types of receptors following inhibition driven by signals from M-cone and S-cone photoreceptors [6, 18, 23]. Elemental colors allow us to distinguish various visible hues in different weighted combinations. Similarly, elemental odors likely are represented in the olfactory third-order neurons and allow us to distinguish various odors in different weighted combinations.

The general principle of odor coding may be identical in humans and mice for basic odors (see Section 3.1). In fact, the helix-8 2nd residues are more than 90% identical (39/42 and 204/226 in class-I and -II, respectively) between human and murine ORs (Table 2). This result also supports the hypothesis that ORs with different residues at the 2nd position of helix 8 play distinct roles in elemental odor representation. We have proposed a hierarchical odor-coding hypothesis (weighted combinatorial receptor codes for elemental odors) for carvone enantiomers (Fig. 3) [6, 18, 22, 23, 38, 39]. In this diagram, the numbers of ORs with the highest sensitivities (four, two, and two ORs for (*R*)-(−)-carvone alone,

(*S*)-(+)-carvone alone, and both (*R*)-(−)- and (*S*)-(+)-carvones, respectively, indicated by the larger symbol) correspond to those observed in an assay of 2740 murine olfactory sensory neurons [38]. Only two of these eight ORs were identified in sequences (car-c5, DDBJ #LC034567; car-n266, DDBJ #LC034578), confirming that they were helix-8-2nd-Glu ORs [6, 23]. This model can explain the consistency of odor percepts during sequential activation of the approximately 70 types (>80% overlapping) of murine ORs responsive to carvone enantiomers; it can also explain unexpected overlapping OR responses to these carvones (sweet, fresh, and herbal odors in humans) and triethylamine (pungent and fishy odors in humans) in 10% of murine carvone ORs [6, 23, 38]. In fact, mice easily distinguish between the (−)- and (+)-enantiomers of carvones over a wide concentration range [23]. In order to analyze odor representation in the brain, we developed a novel wavelet correlation analysis. This analysis revealed a stimulus dependency of oscillatory local field potentials generated in the olfactory third-order neurons, which receive both inhibitory and excitatory signals and the resultant information redundancy changes by integrating multiple cognate OR signals [40]. The olfactory third-order neurons are located in the anterior piriform cortex (aPC, the second olfactory center), where input signals demonstrate an experience dependency [40]. Notably, in the initial phase of odor-induced responses, inhibitory activities are stronger than excitatory activities, resulting in surface-positive local field potentials observed in the aPC [40, 41]. These results support the hierarchical odor-decoding model in which the olfactory system can extract sensory information by summating signals from multiple cognate receptors in the third-order neurons of olfactory pathways via input synchronization through early feedforward inhibition to the pyramidal cells triggered by signals from rapidly activated pairs of key receptors and target G proteins [6, 23].

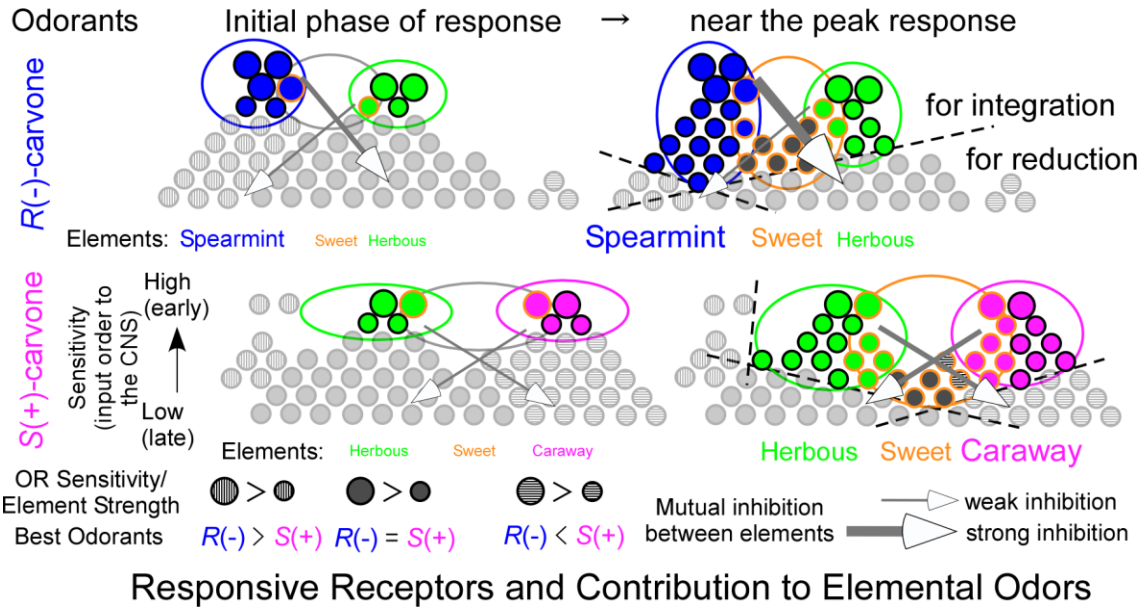

Figure 3. Schematic diagram of hierarchical elemental odor coding (re-used from reference [39]). The hierarchical odor coding scheme selectively ranks dorsal ORs with highest sensitivities (upper side). This establishes a weighted combinatorial receptor code emphasizing unique sensory

qualities (elemental odors, summated signals in large circles) conveyed by the most sensitive dorsal receptors. Based on ranking of olfactory receptor sensitivities, this naturally explains stability of odor quality perception for dose-dependently recruiting receptors over a wide concentration range. The left part represents signals from the most sensitive ORs (color filled circles, each circle size representing signal intensity) and nonresponsive ORs (gray circles) in the initial phase of response. The inhibitory signals trigger synchrony of cognate receptor signal inputs to pyramidal cells that selectively evoke elemental odor percepts. The processing cascade may also act to suppress other odors corresponding to less sensitive (lower side), long latency, and non-cognate ORs near the peak response (on the right side). Primary qualities of odor percepts are determined by the unique elemental odors, and are modulated by secondary qualities from the common odors.

As described in Section 1, the initial, transient, and specific interaction between a GPCR and its target G protein is essential for rapid and robust responses associated with the temporal order of OR signal inputs to the brain. Alanine scanning analysis of *m*OR-S6 helix 8 clearly indicates that the 2nd residue Glu is a major determinant of the initial specific interaction, which is essential for a rapid and robust response, unlike helix-8-2nd-Ala or Lys in ORs or non-target G-proteins [7]. In addition, conserved hydrophobic residues (L/V/A) or Thr at the C-terminal region of TM1 are likely essential to stabilization of the hydrophobic core at the middle region. All nine attested helix-8-2nd-Gln or Asp ORs conserve Gly at this position, which would destabilize the hydrophobic core in the multi-step interactions between ORs and G_{olf} during activation, whereas four of the six attested helix-8-2nd-Glu ORs conserve the L/V/A or Thr residues (Suppl. Fig. S2). As described in Sections 3.2 and 3.3, signals from key helix-8-2nd-Glu dorsal ORs are likely associated with major determinants of the most prominent (upper level) signaling for a given odor (the most prominent elemental odor), whereas helix-8-2nd-Gln and helix-8-2nd-Asp ORs are presumably related to lower levels (auxiliary) of the odor (weaker elemental odors) and/or an enhancement of the most prominent elemental odor [6].

In some cases, destabilization of the hydrophobic core by weak interactions between the helix 8 middle region and TM1 C-terminal Gly partially impairs the rapid activation of the target G protein. In the cases of MAS1 and MAS1L oncogenes, the corresponding sequences markedly and slightly differ, respectively, from those of the other GPCRs (Suppl. Fig. S2), suggesting structural disruptions of helix 8 and the hydrophobic core, as well as their abnormal interactions. Notably, T1Rs and T2Rs are GPCRs that detect sweet, umami, and bitter tastants in heterodimer forms, but do not have the TM3-DRY or TM7-NPxxY motifs or helix 8, suggesting a quite different interaction with their target G protein, gustducin, for sequential activations.

3. Parallel processing for representing elemental odors

3-1. Odor encoding by murine ORs and corresponding human odor qualities.

It is likely that the diversity of OR genes has evolved to distinguish between similar

but slightly different and important olfactory cues comprising similar odorous chemicals and their mixtures. As mentioned earlier, 70% of human ORs have homologous murine ORs. In fact, groupings of murine OR codes for 12 odorants resembled those of human percepts (Fig. 4) [17, 18, 39]. Notably, three response profiles of murine ORs to three distinct subsets of odorants completely matched human odor percepts of vanilla, creamy, and cinnamon. This result is consistent with the widely accepted theory of combinatorial OR coding for odors [26]. However, odorant-characteristic signals from key ORs and their cognate ORs should be emphasized among the more than 80% overlapping carvone ORs for easy discrimination, while signals from the 10% overlapping ORs between dissimilar odors [38] should be reduced or mutually inhibited in a hierarchical manner (Fig. 3). This mechanism is further described in the next section.

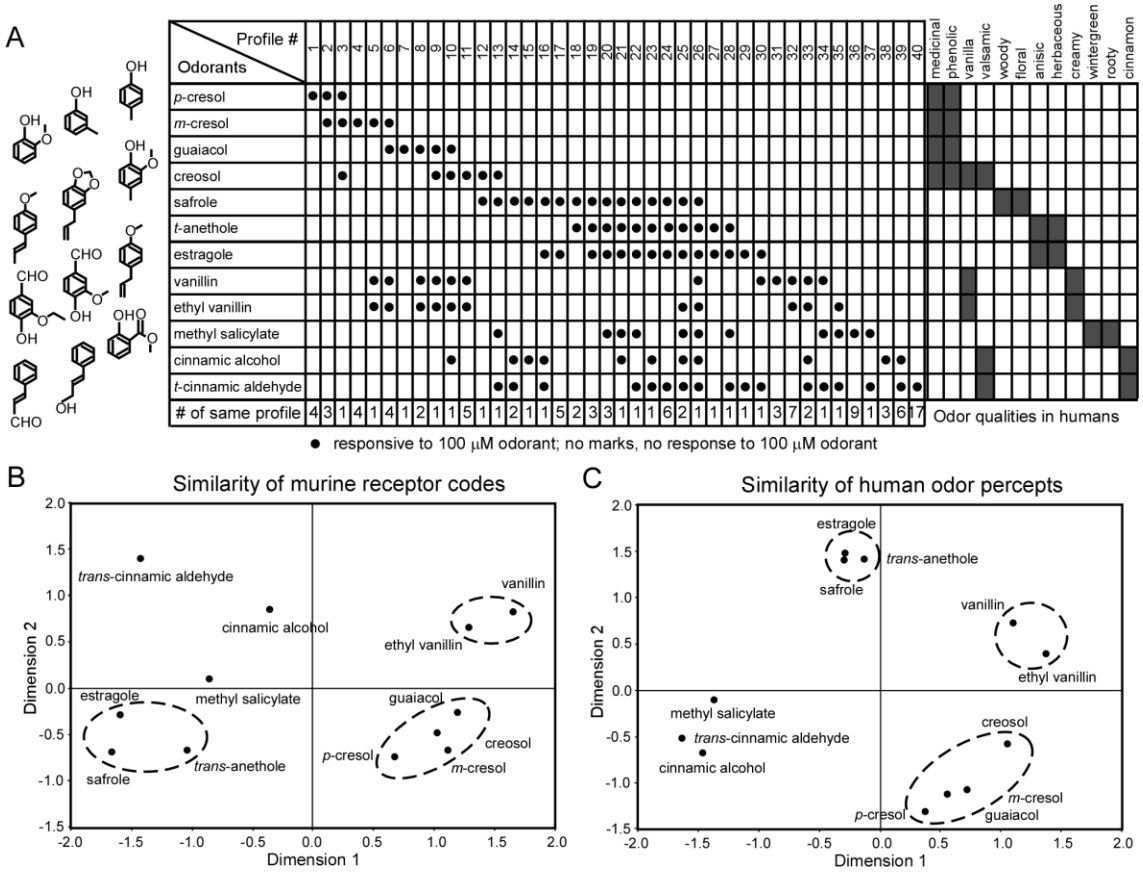

Figure 4. Similarity between murine receptor codes and human odor qualities for 12 odorants (re-used or modified from references [17, 18 & 39]). **A**, Forty different response profiles in murine olfactory sensory neurons and odor qualities in human percepts for 12 odorants. Considering that the sampling rate was 1.1 times for each of 1000 ORs, the number of same profiles would correspond to the number of different ORs with identical response profiles. **B**, Three odorant groups and three independent odorants in murine receptor codes. **C**, Three and one odorant groups that are common to and different from those of murine receptor codes and different from those independency, respectively.

3-2. Emphasis on characteristic elemental odors through feedforward inhibition in the olfactory third-order neurons in the second olfactory center

The sensory profile of an odor stimulus may include several distinct elemental odors if multidimensional input is segmented through parallel pathways [42]. As described above, elemental odors emerge hierarchically through a temporal coding scheme that prioritizes the most sensitive, best-tuned helix-8-2nd-Glu receptors [6, 23]. In this weighted combinatorial receptor-coding (weighted OR signal integration) scheme, feedforward inhibitory signals for input signal synchronization, which are driven by the first-arriving key OR signals in the second olfactory center, are required to integrate signals from key ORs and their cognate ORs for common elements in the olfactory third-order neurons (Fig. 3) [6, 23]. Feedforward inhibition plays a critical role in extracting unique elements by subtracting the overlapping signals between different elements. In the rodent olfactory pathway, feedforward inhibition is activated only in the ventro-rostral portion of the anterior piriform cortex (aPC$_{vr}$) [41] through sensitive pathways via olfactory bulb tufted cells [18, 22, 39, 43]. Notably, in insects, input synchronization via inhibition is also important for discrimination of similar odors [44]. When different stimuli are mixed, our model predicts selective shifts in perceived odors by mutual inhibition to selectively shift the balance of best-tuned sensitive receptors, as is required to distinguish disease-induced body odor disorders (see Section 3.4).

Feedforward inhibition is also associated with mutual inhibition between quite different odors. When wild-type mice recognize the odor of 2,4,5-trimethyl thiazoline (TMT) unique to their predator, the fox, they show freezing behavior with stress responses during which adrenocorticotropic hormone (ACTH) markedly increases in plasma via robust activation of the medial part of the bed nucleus of stria terminals (mBST). However, by genetic ablation of all dorsal ORs, ΔD mice cannot recognize the important TMT odor and exhibit no stress responses [27]. Rose odor alleviates the fox TMT odor-induced stress response in wild-type mice, resulting in no significant increase in plasma ACTH [24], but caraway odor does not [45]. Rose odor mixed with TMT odor reduces the inhibitory signals in the aPC$_{vr}$, but not in the olfactory bulb or the dorsal portion of aPC, compared to those resulting from the TMT odor alone (Fig. 5) [18, 24]. Reduced feedforward inhibition may cause impaired input signal synchrony for TMT ORs and result in decreased intensity of the TMT elemental odor characteristic from the fox. In this model, a hierarchy of elemental odor information processing likely exists in the order rose > TMT > caraway under innate conditions. Familiar odors also reduce stress responses via reduced feedforward inhibition [46]. This suggests that learned relaxation also occurs via reductions in feedforward inhibition of TMT odor recognition.

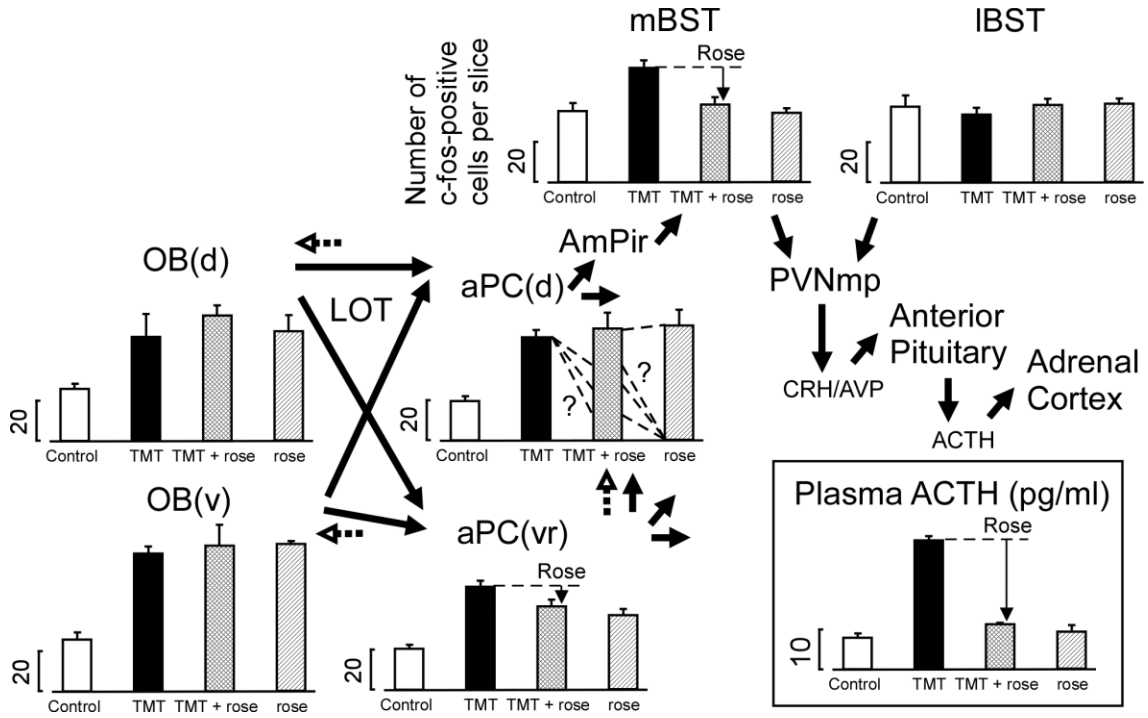

Figure 5. Rose odor alleviates predator odor-induced fear stress through the olfactory pathway (modified from references [18, 24 & 39]). The fox TMT odor activates neurons in the medial part of the bed nucleus of the stria terminalis (mBST), whereas no activity increases were observed in the lateral part of the BST (lBST). Activation of the mBST leads to stress responses in wild-type mice, characterized by an elevated plasma concentration of adrenocorticotropic hormone (ACTH), as shown in the inserted graph. Co-application of rose odor reduced the plasma ACTH concentration and neural activities only in the ventro-rostral part of the anterior piriform cortex (aPC_{vr}) and mBST, compared to those of TMT, while there were no significant differences in both of the dorsal and ventral zones in the olfactory bulb (OB_d, OB_v) and the dorsal part of APC (aPC_d). Arrows indicate signal flows in the olfactory pathway. An open arrow from the aPC_{vr} to the aPC_d and those to the OB indicate feedforward inhibition and efferent inputs for inhibition, respectively. AmPir, amygdalopiriform transition area; AVP, parvocellular arginine vasopressin; CRH, corticotropin-release hormone; LOT, lateral olfactory tract; PVNmp, hypothalamic medial parvocellular paraventricular nucleus. Control means no odor application.

The amygdalopiriform transition area (AmPir) is responsible for the TMT-induced stress response [47]. Interestingly, photo-activated TMT-specific Olfr1019 induces relatively weak immobility behaviors as observed in 1% TMT-treated wild-type mice; 10% TMT-induced immobility was observed in Olfr1019-knockout mice, indicating contribution of other TMT-responsive ORs to the immobility [48]. In addition, photo-activated, TMT-specific Olfr1019 did not induce marked increases in ACTH via robust activation in the mBST, or significant activation in the AmPir. In the weighted OR combinatorial scheme (hierarchical elemental odor-coding scheme), a simple model can explain these results. Among the top five most sensitive ORs to TMT, only Olfr30 is a helix-8-2nd-Glu OR, while the others are helix-8-2nd-Asp ORs. TMT first activates Olfr1019, then Olfr30 among the

helix-8-2nd-Glu ORs, and subsequently signals from Olfr30 induce feedforward inhibition to integrate signals from Olfr1019 and Olfr30 for the TMT-characteristic elemental odor. At less than 1% TMT, signals from Olfr30 may be weak, and integrated signals from Olfr1019 and Olfr30 only induce relatively weak odors, resulting in failure to identify and no aversion to the fox-related odor. At more than 1% TMT, sufficiently intense signals from Olfr30 result in a robust percept of TMT and activations in the AmPir transition area and mBST, as well as robust increases in plasma ACTH and an aversion to the source of TMT. In addition, the destabilization of the hydrophobic core by weakened interaction between the helix-8-middle Met and the TM1 C-terminal Gly (Suppl. Fig. S2) could reduce the response rapidity of Olfr30 as well as those of other TMT ORs (helix-8-2nd-Asp ORs). This model could be confirmed by comparing the robustness of stress responses and feedforward inhibition between sequential photo-activations of Olfr1019 and Olfr30 and its reverse pair.

We considered one possible explanation for the observed hierarchy of elemental odors [6]. In the case that the most sensitive helix-8-2nd-Glu OR to TMT, Olfr30, was less sensitive than the most sensitive helix-8-2nd-Glu OR to rose odor and more sensitive than the most sensitive helix-8-2nd-Glu OR to the caraway elemental odor, rose odor inhibited the elemental odor of TMT and its associated stress responses, suggesting the hierarchy of rose odor > TMT > caraway odor. Notably, innate and learned freezing behaviors are also regulated by hierarchical information processing giving priority to innate signals in the central amygdala [49].

In another example, key ORs for the musk odor were identified in humans and mice by a functional expression assay for all or related subfamily members of ORs [19]. Human OR5AN1, helix-8-2nd-Glu OR, was identified as a key OR for the musk odor. Two homologous ORs in mice, *m*OR215-3 and *m*OR214-4, were found in the GENE database (http://www.ncbi.nlm.nih.gov/gene). Unexpectedly, neither murine ORs responded to 100 μM muscone in the functional expression assay [19, 50]. Interestingly, all three members of the *m*OR215-3 subfamily and all six of the *m*OR214-3 are helix-8-2nd-Glu ORs, and only one member of each subfamily, *m*OR215-1 and *m*OR214-3, were responsive to muscone and other musk odorants [19, 50]. *m*OR215-1 is a dorsal OR and was approximately 10-fold more sensitive to muscone than was *m*OR214-3 in the functional expression assay. The *m*OR215-1-deletion mice displayed 10^2- or 10^3-fold reductions in muscone detection sensitivity compared to that of wild-type mice [19]. These findings support that key ORs in odor representation are helix-8-2nd-Glu ORs (Table 2).

3-3. Odor discrimination paradox by genetic ablation of all dorsal ORs

We conducted two-alternative, forced-choice behavioral assays in a Y-maze to measure odor detection/discrimination thresholds of sniffer mice in a 10- or 100-fold dilution series. A negative pressure-guided odor plume-like flow in the Y-maze enabled us to measure

detection/discrimination thresholds lower than ppq (10^{-15}) levels for single-compound enantiomers [23]. In contrast, transgenic ΔD mice in which all dorsal ORs were ablated displayed a more than 10^{10}-fold reduction in enantiomer discrimination sensitivity, although supersensitive detection of (−)-enantiomers was retained [23]. This result indicates that the most sensitive ventral ORs enabling the transgenic mice to detect (−)-enantiomers but not (+)-enantiomers do not allow the mice to distinguish (−)- from (+)-enantiomers with supersensitivity (odor discrimination paradox, Fig. 6). This suggests that some of the most sensitive and ablated dorsal ORs may be required to enhance detection of characteristic elemental odors in wild-type mice. Among the ablated dorsal ORs, *m*OR-car-c5 is a helix-8-2nd-Glu dorsal OR and one of the most sensitive and specific to (*R*)-(−)-carvone [17]. These results indicate that the highly sensitive helix-8-2nd-Glu dorsal ORs are key ORs in hierarchical elemental odor coding that summate synchronized inputs from cognate ORs to olfactory third-order neurons for elemental odors through feedforward inhibition in the aPC [6].

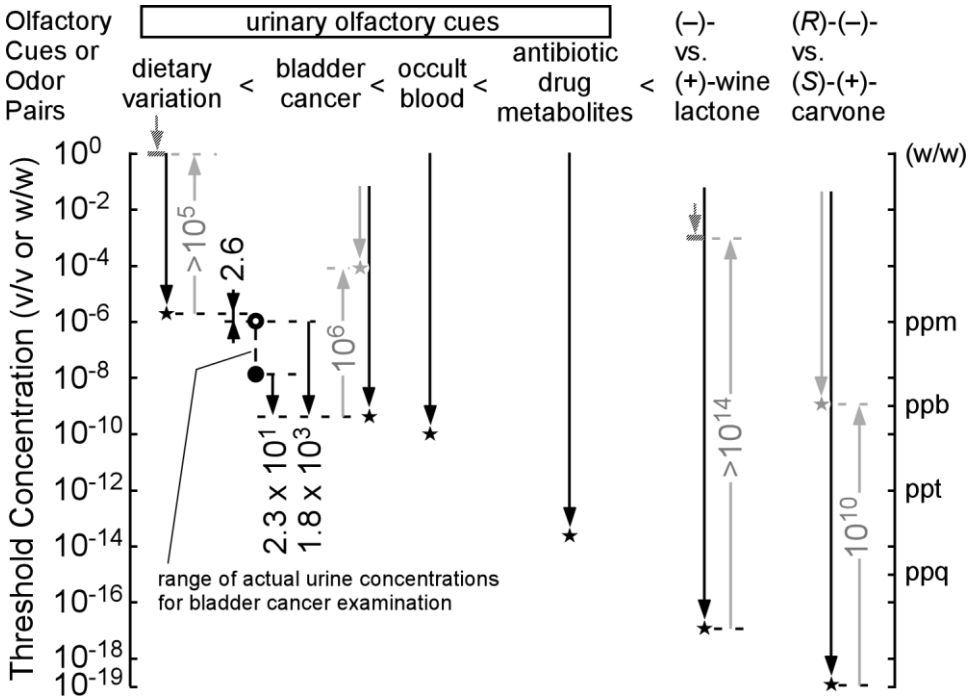

Figure 6. Odor discrimination thresholds of wild-type (WT) and ΔD mice for urinary olfactory cues and enantiomers (re-used from reference [15]). Odor discrimination ranges (downward arrows) and thresholds (stars) of WT (black plots) and ΔD mice (gray plots) for urinary olfactory cues and enantiomer pairs [23] are shown. Odor discrimination thresholds of ΔD mice for dietary variation of body odors and wine-lactone enantiomers are not observed in the concentration ranges examined (hatched arrows), the highest concentrations of which are indicated by the light red bars. Observed threshold differences indicate that urinary olfactory cues increase in the urine mixtures (U_ms) in the following order: dietary variation < bladder cancer < occult blood < antibiotic drug metabolites. The concentration of 10^{-6} v/v (indicated by the black open circle) was used

for bladder cancer examination of individual patient pre-TUR urine samples, as it is the subthreshold for detection of dietary variation in urine and the supra-threshold for detecting bladder cancer odors. Actual concentrations of pre-TUR U_m samples for bladder cancer examination in 10^{-6}-fold diluted equi-occult blood conditions ranged from 10^{-6} v/v (black open circle) to 1.3×10^{-8} v/v (closed circle). ΔD mice exhibited reduced odor discrimination sensitivities compared to WT mice; degrees of sensitivity reduction due to ablation of dorsal olfactory receptors are indicated by the gray upward arrows.

3-4. Detection of bladder cancer-induced urine odor disorder

We recently reported that sniffer mice can distinguish between urine odor changes in patients with bladder cancer in a 10^{-6}-fold diluted condition, 2.6-fold below the detection level of dietary and/or inter-individual variations, at equal concentrations of occult blood in Y-maze behavioral assays [15]. To reduce dietary and inter-individual variations, we employed urine mixtures (U_m) of 5 to 25 samples. In the U_m, urinary olfactory cues of body odor increased in the following order: dietary variation < bladder cancer < occult blood < antibiotic drug metabolites (Fig. 6) [15]. This provided a biological basis for detection of body odor disorders in U_m conditions for non-invasive diagnostic tests for cancers or other diseases. The sniffer mice achieved a success rate of 100% for the individual urine samples of 11 patients with or without occult blood according to memory-based odor discrimination ability in the Y-maze assay [15].

The greater intensity of urinary occult blood olfactory cues compared to genetically determined body odors is consistent with the previous observation that body odor discrimination is more difficult in serum than in urine samples [51]. In addition, the observation that cadaver dogs can detect different human blood samples even at very low concentrations [52] suggests a salient olfactory cue common across individual blood samples. A volatile chemical *trans*-4,5-epoxy-(E)-2-decenal presents an intense odor characteristic of blood samples [53] through lipid peroxidation [54] as an olfactory cue of the occult blood. These results emphasize the excellent ability of dogs and mice to distinguish weak but biologically important olfactory cues over those of abundant compounds. In the next study, the accuracy of the test across various cases will be examined as well as the recurrence risk of bladder and other types of cancers.

Future analysis of urine mixtures may provide more robust biomarkers than those of individual urine samples, which vary at relative concentrations of diet- and genetically determined body odor-related compounds. As the signal averaging of replicate measures improves signal-to-noise ratio, mixing replicate urine samples from several patients with bladder cancer would establish concentration profiles of compounds common to multiple urine samples and reduce relative concentrations of variable compounds. This would also reduce possible synergistic or antagonistic effects of relatively dilute variable compounds on bladder cancer-related odors in the urine sample mixtures. Currently available analytical instruments, such as gas chromatography-mass spectroscopy (GC-MS) systems [55–59] and electronic-nose (e-nose)

devices [60–65], are generally less sensitive to the different profiles of trace key compounds in body odors than are murine or canine olfactory systems [15]. However, by identifying the trace and abundant key compounds in urine mixtures that occur due to diseases, such as bladder cancer, we may be able to determine novel molecular biomarkers for non-invasive disease diagnosis.

Our results also indicate a possible mechanism underlying the olfactory discrimination of bladder cancer-induced urine odor changes and healthy odors. Body odors may evoke similar, yet distinct, odor perceptions through nonlinear contributions of multiple olfactory receptors activated by multiple odorous compounds. Considering that no diet-specific or tumor-specific odorous compounds appear in solid phase microfiber extraction-gas chromatography-mass spectroscopy profiles [10, 11], it is difficult to explain the easy discrimination of weaker identical olfactory cues [10, 15] or similar odors for more than 80% overlapping ORs [38] under the conventional olfactory coding scheme based on simple combinatorial representation of different odors by different subsets of responsive olfactory receptors [26]. When some urinary odorants slightly change due to metabolic disorders in tumors, the earliest signals arriving from the most sensitive, short-latency, helix-8-2nd-Glu dorsal ORs are altered. The early inhibitory signals also change, subsequently altering cognate receptor signal inputs to pyramidal cells and their input synchronization for signal integration via feedforward inhibition. This selectively evokes "elemental" odor perceptions by engaging associated neural pathways, thereby changing the elemental odor hierarchy.

We found that ΔD mice showed at least a 10^5-fold reduction in discrimination sensitivity for body odors, indicating an essential role of the ablated dorsal ORs in body odor recognition [15]. This reduction is almost half the 10^{10}-fold reduction in carvone enantiomer discrimination sensitivity (Fig. 6) [15]. This difference is likely attributable to a greater number of key olfactory receptors for multiple-compound body odors and/or a major contribution of class-I olfactory receptors that are all dorsal receptors, as olfactory receptors for single-compound wine lactone or carvone enantiomers are fewer in number than those for body odors and are mainly class-II olfactory receptors [23]. Class-II ORs are likely associated with increased detection sensitivities.

4. Future directions

As observed in genetic variant CX3CR1-A55T, destabilization of the hydrophobic core between GPCR helix 8 and TM1–2 could cause diseases mediated by impaired GPCR signaling pathways. Taken together with our observation that GPCR helix-8-2nd-residue mutation impairs rapid and specific interactions with target G proteins, various associations between GPCRs and diseases may be potential drug targets. Regarding the olfactory system, based on weighted combinatorial receptor coding [23], minor changes in intensity profiles of dorsal ORs drive changes in the elemental odor hierarchy, which occurs more easily in olfactory systems using greater repertoires of ORs, such as in mice, even if the combinations of activated ORs are identical. Further investigations are needed to determine

whether all helix-8-2nd-Glu ORs function as key ORs, namely, as determinants of the most prominent elemental odors, and whether either of helix-8-2nd-Asp ORs or helix-8-2nd-Gln ORs are determinants of auxiliary elemental odors or the most prominent elemental odors under specific conditions. The mechanism by which humans and mice recognize odor uniqueness and similarity also warrants further examination. These determinations would enable us to understand the genetic strategy of GPCR parallel signaling systems for recognition of important sensory cues.

List of abbreviations

ACTH, adrenocorticotropic hormone; AmPir, amygdalopiriform transition area; β_2AdR, β_2 adrenergic receptor; CX3CR1, C-X3-C motif chemokine receptor 1; e-nose, electronic-nose; EC, extracellular loop; FSH, follicle-stimulating hormone; GPCR, G protein-coupled receptor; GC-MS, gas chromatography-mass spectroscopy; 5-HT, 5-hydroxytryptamine; IC, intracellular loop; LH, luteinizing hormone; mBST, the medial part of the bed nucleus of stria terminals; M3R, M3 muscarinic acetylcholine receptor; ORs, olfactory receptors; TM, transmembrane domain; TMT, 2,4,5-trimethyl thiazoline; TSH, thyroid-stimulating hormone; U_m, urine mixtures; aPC_{vr}, the ventro-rostral portion of the anterior piriform cortex.

References

1. Bjarnadóttir TK, Gloriam DE, Hellstrand SH, Kristiansson H, Fredriksson R, Schiöth HB. Comprehensive repertoire and phylogenetic analysis of the G protein-coupled receptors in human and mouse. *Genomics* 2006;88:263−273.

2. Overington JP, Al-Lazikani B, Hopkins AL. How many drug targets are there? *Nat. Rev.* 2006;5:993–996.

3. Wang W, Qiao Y, Li Z. New insights into modes of GPCR activation. *Trends Pharmacol. Sci.* 2018;39:367–386. doi: 10.1016/j.tips.2018.01.001.

4. Hauser AS, Chavali S, Masuho I, Jahn LJ, Martemyanov KA, Gloriam DE, Babu MM. Pharmacogenomics of GPCR drug targets. *Cell* 2018;172:41–54.e19. doi: 10.1016/j.cell.2017.11.033.

5. Flock T, Hauser AS, Lund N, Gloriam DE, Balaji S, Babu MM. Selectivity determinants of GPCR-G-protein binding. *Nature* 2017;545:317–322. doi: 10.1038/nature22070.

6. Sato T, Kawasaki T, Mine S, Matsumura H. Functional role of the C-terminal amphipathic helix 8 of olfactory receptors and other G protein-coupled receptors. *Int. J. Mol. Sci.* 2016;17:pii:E1930. doi: 10.3390/ijms17111930.

7. Kawasaki T, Saka T, Mine S, Mizohata E, Inoue T, Matsumura H, Sato T. The N-terminal acidic residue of the cytosoloc helix 8 of an odorant receptor is responsible for different response dynamics via G-protein. *FEBS Lett.* 2015;589:1136−1142.

8. Ballister ER, Rodgers J, Martial F, Lucas RJ. A live cell assay of GPCR coupling allows identification of opto-

genetic tools for controlling G_o and G_i signaling. *BMC Biol.* 2018;16:10. doi: 10.1186/s12915-017-0475-2.

9. Schaefer ML, Yamazaki K, Osada K, Restrepo D, Beauchamp GK. Olfactory fingerprints for major histocompatibility complex-determined body odors II: relationship among odor maps, genetics, odor composition, and behavior. *J. Neurosci.* 2002;22:9513–9521.

10. Kwak J, Willse A, Matsumura K, Curran Opiekun M, Yi W, Preti G, Yamazaki K, Beauchamp GK. Genetically-based olfactory signatures persist despite dietary variation. *PLoS One* 2008;3:e3591.

11. Matsumura K, Opiekun M, Oka H, Vachani A, Albelda SM, Yamazaki K, Beauchamp GK. Urinary volatile compounds as biomarkers for lung cancer: a proof of principle study using odor signatures in mouse models of lung cancer. *PLoS One* 2010;5:e8819.

12. Willis CM, Church SM, Guest CM, Cook WA, McCarthy N, Bransbury AJ. Olfactory detection of human bladder cancer by dogs: proof of principle study. *BMJ* 2004;40:321–323.

13. McCulloch M, Jezierski T, Broffman M, Hubbard A, Turner K, Janecki T. Diagnostic accuracy of canine scent detection in early- and late-stage lung and breast cancers. *Integr. Cancer Ther.* 2006;5:30–39.

14. Boedeker E, Friedel G, Walles T. Sniffer dogs as part of a bimodal bionic research approach to develop a lung cancer screening. *Interact. Cardiovasc. Thorac. Surg.* 2012;14:511–515.

15. Sato T, Katsuoka Y, Yoneda K, Nonomura M, Uchimoto S, Kobayakawa R, Kobayakawa K, Mizutani Y. Sniffer mice discriminate urine odors of patients with bladder cancer: A proof-of-principle study for non-invasive diagnosis of cancer-induced odors. *Sci. Rep.* 2017;7:14628. https://www.nature.com/articles/s41598-017-15355-z

16. Niimura Y, Matsui A, Touhara K. Extreme expansion of the olfactory receptor gene repertoire in African elephants and evolutionary dynamics of orthologous gene groups in 13 placental mammals. *Genome. Res.* 2014;24:1485–1496.

17. Furudono Y, Sone Y, Takizawa K, Hirono J, Sato T. Relationship between peripheral receptor code and perceived odor quality. *Chem. Senses* 2009;31:151–159, doi: 10.1093/chemse/bjn071.

18. Sato T, Matsukawa M, Furudono Y, Hirono J, Emura M. Olfactory pathway for stress relaxation and sensory basis for olfactory-compatible sensors. In Tonoike M. (ed.), *Flavors and five senses*, Tokyo, Fregrance Journal Ltd. 2016;164–181 (Japanese).

19. Sato-Akuhara N, Horio N, Kato-Namba A, Yoshikawa K, Niimura Y, Ihara S, Shirasu M, Touhara K. Ligand specificity and evolution of mammalian musk odor receptors: effect of single receptor deletion on odor detection. *J. Neurosci.* 2016;36:4482–4491.

20. Mombaerts P, Wang F, Dulac C, Chao SK, Nemes A, Mendelsohn M,

Edmondson J, Axel R. Visualizing an olfactory sensory map. *Cell* 1996;87:675–686.

21. Serizawa S, Miyamichi K, Takeuchi H, Yamagishi Y, Suzuki M, Sakano H. A neuronal identity code for the odorant receptor-specific and activity-dependent axon sorting. *Cell* 2006;127:1057–1069

22. Sato T, Hirono J, Hamana H, Ishikawa T, Shimizu A, Takashima I, Kajiwara R, Iijima T. Architecture of odor information processing in the olfactory system. *Anat. Sci. Int.* 2008;83:195–206, doi: 10.1111/j.1447-073X.2007.00215.x.

23. Sato T, Kobayakawa R, Kobayakawa K, Emura M, Itohara S, Kizumi M, Hamana H, Tsuboi A, Hirono J. Supersensitive detection and discrimination of enantiomers by dorsal olfactory receptors: evidence for hierarchical odour coding. *Sci. Rep.* 2015;5:14073. https://www.nature.com/articles/srep14073

24. Matsukawa M, Imada M, Murakami T, Aizawa S, Sato T. Rose odor can innately counteract predator odor. *Brain Res.* 2011;1381:117–123.

25. Serizawa S, Miyamichi H, Sakano H. One neuron-one receptor rule in the mouse olfactory system. *Trends Genet.* 2004;20:648–653.

26. Malnic B, Hirono J, Sato T, Buck L. Combinatorial receptor codes for odors. *Cell* 1999;96:713–723.

27. Kobayakawa K, Kobayakawa R, Matsumoto H, Oka Y, Imai T, Ikawa M, Okabe M, Ikeda T, Itohara S, Kikusui T, Mori K, Sakano H. Innate versus learned odour processing in the mouse olfactory bulb. *Nature* 2007;450:503–508.

28. Rasmussen SG, DeVree BT, Zou Y, Kruse AC, Chung KY, Kobilka TS, Thian FS, Chae PS, Pardon E, Calinski D, Mathiesen JM, Shah ST, Lyons JA, Caffrey M, Gellman SH, Steyaert J, Skiniotis G, Weis WI, Sunahara RK, Kobilka BK. Crystal structure of the β_2 adrenergic receptor-G_s protein complex. *Nature* 2011;477:549−555.

29. Huang W, Manglik A, Venkatakrishnan AJ, Laeremans T, Feinberg EN, Sanborn AL, Kato HE, Livingston KE, Thorsen TS, Kling RC, Granier S, Gmeiner P, Husbands SM, Traynor JR, Weis WI, Steyaert J, Dror RO, Kobilka BK. Structural insights into μ opioid receptor activation. *Nature* 2015;524:315−321.

30. Venkatakrishnan AJ, Deupi X, Lebon G, Heydenreich FM, Flock T, Miljus T, Balaji S, Bouvier M, Veprintsev DB, Tate CG, Schertler GF, Babu MM. Diverse activation pathways in class A GPCRs converge near the G-protein-coupling region. *Nature* 2016;536:484−487.

31. Ballesteros JA, Weinstein H. Integrated methods for the construction of three-dimensional models and computational probing of structure-function relations in G protein-coupled receptors. *Method. Neurosci.* 1995;25:366−428.

32. Fritze O, Filipek S, Kuksa V, Palczewski K, Hofmann KP, Ernst OP. Role of the conserved NPxxY(x)5,6F motif in the rhodopsin ground state and during activation. *Proc. Natl. Acad. Sci. U.S.A.* 2003;100:2290−2295.

33. Cherezov V, Rosenbaum DM, Hanson MA, Rasmussen SG, Thian FS, Kobilka TS, Choi HJ, Kuhn P, Weis WI, Kobilka BK, Stevens RC. High-resolution crystal structure of an engineered human β_2-adrenergic G protein-coupled receptor. *Science* 2007;318:1258−1265.

34. Palczewski K, Kumasaka T, Hori T, Behnke CA, Motoshima H, Fox BA, Le Trong I, Teller DC, Okada T, Stenkamp RE, Yamamoto M, Miyano M. Crystal structure of rhodopsin: A G protein-coupled receptor. *Science* 2000;289:739−745.

35. Ishizuka K, Fujita Y, Kawabata T, Kimura H, Iwayama Y, Inada T, Okahisa Y, Egawa J, Usami M, Kushima I, Uno Y, Okada T, Ikeda M, Aleksic B, Mori D, Someya T, Yoshikawa T, Iwata N, Nakamura H, Yamashita T, Ozaki N. Rare genetic variants in *CX3CR1* and their contribution to the increased risk of schizophrenia and autism spectrum disorders. *Transl Psychiatry* 2017;7:e1184. doi: 10.1038/tp.2017.173.

36. Hu J, Wang Y, Zhang X, Lloyd JR, Li JH, Karpiak J, Costanzi S, Wess J. Structural basis of G protein-coupled receptor-G protein interactions. *Nat. Chem. Biol.* 2010;6:541−548.

37. Vohra S, Taddese B, Conner AC, Poyner DR, Hay DL, Barwell J, Reeves PJ, Upton GJ, Reynolds CA. Similarity between class A and class B G-protein-coupled receptors exemplified through calcitonin gene-related peptide receptor modelling and mutagenesis studies. *J. R. Soc. Interface* 2012;10:20120846. http://rsif.royalsocietypublishing.org/content/10/79/20120846.long

38. Hamana H, Hirono J, Kizumi M, Sato T. Sensitivity-dependent hierarchical receptor codes for odors. *Chem. Senses* 2003;28:87–104.

39. Sato T, Matsukawa M, Furudono Y. Algorithm of odor information processing. Oyo-Butsuri 2014 83:43–47 (Japanese).

40. Sato T, Kajiwara R, Takashima I, Iijima T. A novel method for quantifying similarities between oscillatory neural responses in wavelet time-frequency power profiles. *Brain Res.* 2016;1636:107–117.

41. Ishikawa T, Sato T, Shimizu A, Tsutsui K, de Curtis M, Iijima T.Odor-driven activity in the olfactory cortex of an in vitro isolated guinea pig whole brain with olfactory epithelium. *J. Neurophysiol.* 2007;97:670–679.

42. Rokin D, Hemmelder V, Kapoor V, Murthy VN. An olfactory cocktail party: figure-ground segregation of odorants in rodents. *Nat. Neurosci.* 2014;17:1225–1232.

43. Igarashi KM, Ieki N, An M, Yamaguchi Y, Nagayama S, Kobayakawa K, Kobayakawa R, Tanifuji M, Sakano H, Chen WR, Mori K. Parallel mitral and tufted cell pathways route distinct odor information to different targets in the olfactory cortex. *J. Neurosci.* 2012;32:7870–7885, doi: 10.1523/JNEUROSCI.0154-12.2012.

44. Stopfer M, Bhagavan S, Smith BH, Laurent G. Impaired odour discrimination on desynchronization of odour-encoding neural assemblies. *Nature* 1997;390:70−74.

45. Murakami T, Matsukawa M, Katsuyama N, Imada M, Aizawa S, Sato T. Stress-related activities induced by predator odor may become indistinguishable by hinokitiol odor. *Neuroreport* 2012;23:1071–1076.

46. Matsukawa M, Imada M, Aizawa S, Sato T. Habitat odor can alleviate innate stress responses in mice. *Brain Res.* 2016;1631:46–52. doi: 10.1016/j.brainres.2015.11.020.

47. Kondoh K, Lu Z, Ye X, Olson DP, Lowell BB, Buck LB. A specific area of olfactory cortex involved in stress hormone responses to predator odours. *Nature* 2016;532:103–106. doi: 10.1038/nature17156.

48. Saito H, Nishizumi H, Suzuki S, Matsumoto H, Ieki N, Abe T, Kiyonari H, Morita M, Yokota H, Hirayama N, Yamazaki T, Kikusui T, Mori K, Sakano H. Immobility responses are induced by photoactivation of single glomerular species responsive to fox odour TMT. *Nat Commun.* 2017;8:16011. doi: 10.1038/ncomms16011.

49. Isosaka T, Matsuo T, Yamaguchi T, Funabiki K, Nakanishi S, Kobayakawa R, Kobayakawa K. Htr2a-expressing cells in the central amygdala control the hierarchy between innate and learned fear. *Cell* 2015;163:1153–1164. doi: 10.1016/j.cell.2015.10.047.

50. Shirasu M, Yoshikawa K, Takai Y, Nakashima A, Takeuchi H, Sakano H, Touhara K. Olfactory receptor and neural pathway responsible for highly selective sensing of musk odors. *Neuron* 2014;81:165–178.

51. Yamazaki K, Beauchamp GK, Singer A, Bard J, Boyse EA. Odortypes: their origin and composition. *Proc. Natl. Acad. Sci. U.S.A.* 1999;96:1522–1525.

52. Riezzo I, Neri M, Rendine M, Bellifemina A, Cantatore S, Fiore C, Turillazzi E. Cadaver dogs: unscientific myth or reliable biological devices? *Forensic. Sci. Int.* 2014;244:213–223, doi: 10.1016/j.forsciint.2014.08.026.

53. Arshamian A, Laska M, Gordon AR, Norberg M, Lahger C, Porada DK, Jelvez Serra N, Johansson E, Schaefer M, Amundin M, Melin H, Olsson A, Olsson MJ, Stensmyr M, Lundström JN. A mammalian blood odor component serves as an approach-avoidance cue across phylum border - from flies to humans. *Sci. Rep.* 2017;7:13635. doi: 10.1038/s41598-017-13361-9.

54. Buettner A, Schieberle P. Aroma properties of a homologous series of 2, 3-epoxyalkanals and trans-4, 5-epoxyalk-2-enals. *J. Agric. Food Chem.* 2001;49:3881–3884.

55. Silva CL, Passos M, Câmara JS. Investigation of urinary volatile organic metabolites as potential cancer biomarkers by solid-phase microextraction in combination with gas chromatography-mass spectrometry. *Br. J. Cancer* 2011;105:1894–1904.

56. Hanai Y, Shimono K, Matsumura K, Matsumura K, Vachani A, Albelda S, Yamazaki K, Beauchamp GK, Oka H. Urinary volatile compounds as biomarkers for lung cancer. *Biosci. Biotechnol. Biochem.* 2012;76:679–684.

57. Jobu K, Sun C, Yoshioka S, Yokota J, Onogawa M, Kawada C, Inoue K, Shuin T, Sendo T, Miyamura M. Meta-

bolomics study on the biochemical profiles of odor elements in urine of human with bladder cancer. *Biol. Pharm. Bull.* 2012;35:639–642.

58. Fischer S, Bergmann A, Steffens M, Trefz P, Ziller M, Miekisch W, Schubert JS, Köhler H, Reinhold P. Impact of food intake on in vivo VOC concentrations in exhaled breath assessed in a caprine animal model. *J. Breath Res.* 2015;9:047113: http://iopscience.iop.org/article/10.1088/1752-7155/9/4/047113/meta;jsessionid=9BED5B4171BA49AEF7A04E2E1087B167.c2.iopscience.cld.iop.org.

59. Fischer S, Trefz P, Bergmann A, Ziller M, Miekisch W, Schubert JS, Köhler H, Reinhold P. Physiological variability in volatile organic compounds (VOCs) in exhaled breath and released from faeces due to nutrition and somatic growth in a standardized caprine animal model. *J. Breath Res.* 2015;9:027108: http://iopscience.iop.org/article/10.1088/1752-7155/9/2/027108/meta.

60. Wilson AD. Recent progress in the design and clinical development of electronic-nose technologies. *Nanobiosensors in Disease Diagnosis* 2016;5:15–27: https://www.dovepress.com/recent-progress-in-the-design-and-clinical-development-of-electronic-n-peer-reviewed-article-NDD .

61. Horvath G, Chilo J, Lindblad T. Different volatile signals emitted by human ovarian carcinoma and healthy tissue. *Future Oncol.* 2010;6:1043–1049.

62. Shehada N, Brönstrup G, Funka K, Christiansen S, Leja M, Haick H. Ultrasensitive silicon nanowire for real-world gas sensing: noninvasive diagnosis of cancer from breath volatolome. *Nano Lett.* 2015;15:1288–1295.

63. Mazzatenta A, Pokorski M, Di Tano A, Cacchio M, Di Giulio C. Influence of sensory stimulation on exhaled volatile organic compounds. *Adv. Exp. Med. Biol.* 2016;884:75–79.

64. Mazzatenta A, Pokorski M, Di Giulio C. Real time analysis of volatile organic compounds (VOCs) in centenarians. *Respir. Physiol. Neurobiol.* 2015;209:47–51.

65. Mazzatenta A, Pokorski M, Sartucci F, Domenici L, Di Giulio C. Volatile organic compounds (VOCs) fingerprint of Alzheimer's disease. *Respir. Physiol. Neurobiol.* 2015;209:81–84.

Acknowledgements

This study was supported by a Grant-in-Aid for Scientific Research (B) #15H02730 (T.S.).

Author Contributions

All authors discussed about interpretation of data. The manuscript was written by T.S., M.M. and H.M.

Competing Financial Interests

The authors declare no competing financial interests.

Supplementary Materials

Initial, transient, and specific interaction between G protein-coupled receptor and target G protein in parallel signal processing: a case of olfactory discrimination of cancer-induced odors

Takaaki Sato*[1], Mutsumi Matsukawa[2], Yoichi Mizutani[3], Toshio Iijima[4] and Hiroyoshi Matsumura[5]

[1]Biomedical Research Institute, National Institute of Advanced Industrial Science and Technology, Osaka, Japan; [2]Division of Anatomical Science, Department of Functional Morphology, Nihon University School of Medicine, Tokyo, Japan; [3]Department of Medical Engineering, Faculty of Health Science, Aino University, Osaka, Japan; [4]Graduate School of Life Sciences, Tohoku University, Sendai, Japan; [5]College of Life Sciences, Ritsumeikan University, Kusatsu, Japan

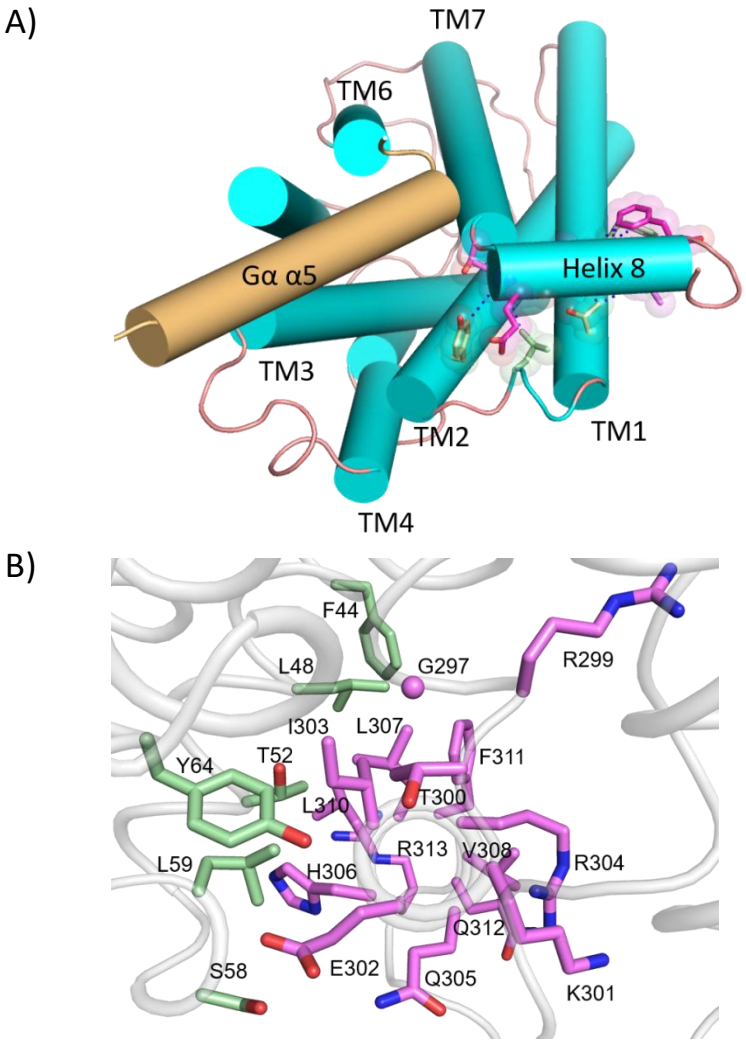

Supplementary Fig. S1. A homology-modeled *m*OR-S6 based on an active-state β_2 adrenergic receptor (from Reference [3] with modification). **A**) Cytoplasmic view with residues for hydrophobic core and helix-8-2nd residue. **B**) A helix-8 N-terminal front view of detailed interfaces of helix 8 and TM1–2.

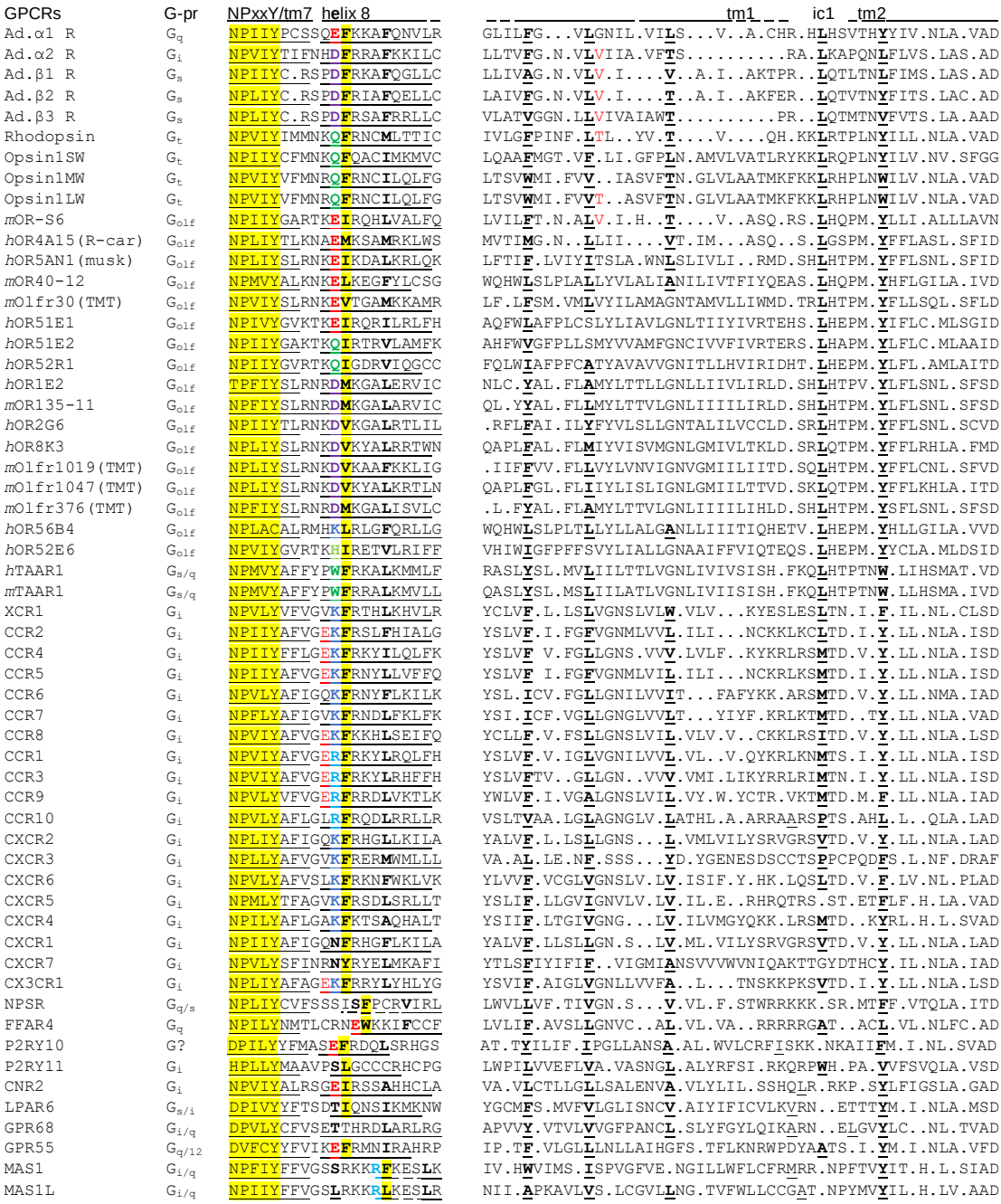

Supplementary Fig. S2. Alignment of amino acid sequences of NPxxY motif, helix 8, and TM1–IC1–TM2 of GPCRs. The 38 human non-olfactory GPCRs and 19 ORs/TAARs with their target G proteins (from http://www.guidetopharmaco logy.org) are shown. Lys of the NPxxY motif interacts with helix-8 **3rd residue** in the inactive state but not in the active state. In the active state, **hydrophobic residues** at the helix-8 **3rd**, **7th**, 10th, and 11th positions interact with **hydrophobic residues** conserved at the middle region of IC1, the C-terminal and N-terminal regions of TM1 (tm1) and TM2 (tm2), respectively. Neuropeptides S receptor (NPSR) and free fatty acid receptor 4 (FFAR4) may cause a shift in the position of helix 8 by two amino acids. Helix 8 of MAS1, MAS1L, and NPSR are likely to be unstable. Ad $\alpha_{1/2}/\beta_{1/2/3}$ R, adrenergic $\alpha_{1/2}/\beta_{1/2/3}$ receptor; Opsin1SW/MW/LW, opsin1, short/middle/long wavelength sensitive; *h*/*m*OR, human/murine olfactory receptor; *m*Olfr, murine olfactory receptor; *h*/*m*TAAR, human/murine trace amine-associated receptor; XCR1, chemokine (C) receptor; CCR1–10, chemokine (C–C) receptor 1–10; CXCR1–7, chemokine (C-X-C) receptor 1–7; CX3CR1, chemokine (C-X3-C) receptor 1; P2RY10/11, purinergic P2Y10/11 receptor; CNR2, cannabinoid receptor 2; LPAR6, lysophosphatidic acid receptor 6; GPR68/55, orphan class A15 receptor 68/55; MAS1, MAS1 proto-oncogene G protein-coupled receptor; MAS1L, MAS1 proto-oncogene like, G protein-coupled receptor.

Human ORs			Homologous murine ORs			Subclass
mOR-S6	*TM7-NPxxY*	*helix 8*	*mOR-S6*	*TM7-NPxxY*	*helix 8*	
			*m*OR-S6	NPIIYGARTK**E**IRQHLVALFQ		
*h*OR51A7	NPIVYCVKTR**Q**IWEKILGKLL		*m*OR8-5	NPIVYCIKTR**Q**IREKVLGKLV		class I OR
*h*OR51B2	NPVIYSIKTK**Q**IQYGIIRLLS		*m*OR1-1	NPIIYSIKTK**Q**IQRSVLRLLS		
*h*OR51B4	NPIIYSIKTK**Q**IQRSIIRLFS		*m*OR1-3	NPIIYSIKTK**Q**IQRSVLRLLS		
*h*OR51B6	NPFIYSIKTK**Q**IQSGILRLFS		*m*OR1-2	NPVIYSIKTK**Q**IQSGLLRLFS		
*h*OR51D1	NPLVYGAKTK**E**ICSRVLCMFS		*m*OR18-3	NPIVYGAKTK**E**IRSRVIRMFS		
*h*OR51E1	NPIVYGVKTK**E**IRQRILRLFH		*m*OR18-1	NPIVYGVKTK**E**IRQRILRLFL		
*h*OR51E2	NPIIYGAKTK**Q**IRTRVLAMFK		*m*OR18-2	NPIIYGAKTK**Q**IRTRVLAMFK		
*h*OR51F2	NPIIYSVKIK**Q**IQKAIIKVLI		*m*OR14-3	NPIIYSVKIK**Q**IQKAIIKVLI		
*h*OR51G1	NPIIYSIKTK**Q**IRQRIIKKFQ		*m*OR7-1	NPIVYSIKTK**Q**IRQRIIKKFE		
*h*OR51G2	NPIVYSVKTK**Q**IRDRVTHAFC		*m*OR7-2	NPIVYSVKTK**Q**IRDRVAHAFC		
*h*OR51I1	NPIIYSVKTK**E**IRKGILKFFH		*m*OR13-4	NPIIYSVKTK**E**IRKGMLKVFH		
*h*OR51I2	NPLIYSAKTK**E**IRRAIFRMFH		*m*OR13-3	NPLIYSAKTK**E**IRRAIFRMFR		
*h*OR51M1	NPIIYSIKTK**E**IHRAIIKFLG		*m*OR3-1	NPVIYSIKTK**E**IRKAIIRFLG		
*h*OR51Q1	NPIIYSVKNK**Q**IQWGMLNFLS		*m*OR5-1	NPIIYSVKTK**Q**IRQGITRLLL		
*h*OR51S1	NPILYSVKMK**E**IRKRILNRLQ		*m*OR21-1	NPVLYSVKMK**E**IREKILKRLL		
*h*OR51T1	NPIIYSLKTK**T**IRQAMFQLLQ		*m*OR14-9	NPIIYSLKTK**V**IRQAIFQLFR		
*h*OR52A1	NPLVYGAKTT**Q**IRIHVVKMFC		*m*OR22-3	NPIVYGVKTK**Q**IRDQVLKMLF		
*h*OR52A5	NPIVYGVKTK**Q**IRDHIVKVFF		*m*OR22-2	NPIVYGVKTK**Q**IRDQVLKMLF		
*h*OR52B2	NPIVYGVKTK**Q**IREGVAHRFF		*m*OR31-6	NPIVYGVKTK**Q**IREGVVHWFL		
*h*OR52B4	NPIIYGIKTK**Q**IQEQVVQFLF		*m*OR31-4	NPIIYGIKTK**Q**IQEQMVHVLF		
*h*OR52B6	NPVIYGVRTK**P**ILEGAKQMFS		*m*OR31-9	NPIIYGVKTK**Q**IQDRFFQLFS		
*h*OR52D1	NPILYGARTK**E**IRSRLLKLLH		*m*OR33-2	NPIIYGARTK**E**IRSRLLKLLH		
*h*OR52E2	NPVIYGVRTK**Q**IYKCVKKILL		*m*OR32-10	NPVIYGVRTK**Q**IYDRVKKIFL		
*h*OR52E4	NPVIYGVRTK**Q**IREQIVKIFV		*m*OR32-11	NPVIYGVRTK**Q**IREKIIKIVV		
*h*OR52E8	NPVIYGVRTK**Q**IRERVLRIFL		*m*OR32-9	NPVIYGVRTK**Q**IREQVMRILF		
*h*OR52H1	NPMVYGVKTK**Q**IRDKVILLFS		*m*OR31-12	NPIVYGVKTK**Q**IREKVILLFS		
*h*OR52I2	NPIIYGMRTK**Q**LRERIWSYLM		*m*OR41-1	NPIIYGIRTR**Q**IRERIWSLLT		
*h*OR52J3	NPIIYGVRTK**Q**IRERVLYVFT		*m*OR32-13	NPIIYSVRTK**Q**IREHVLHIFT		
*h*OR52K2	NPIIYGVKTK**Q**IRESILGVFP		*m*OR28-1	NPIIYGVKTK**Q**IRERVLGLFL		
*h*OR52L1	NPLVYGVKTQ**Q**IRQRVLRVFT		*m*OR37-1	NPLVYGVKTR**Q**IRQRVLRVFY		
*h*OR52M1	NPIVYAVRTK**Q**IRESLLQIPR		*m*OR25-1	NPIVYAVRTK**Q**IRDRLLQILK		
*h*OR52N1	NPIVYGVKTR**Q**VRESVIRFFL		*m*OR34-6	NPIVYGMKTK**Q**IRDSIIKFFH		
*h*OR52N2	NPIVYGVKTK**Q**IQEGVIKFLL		*m*OR34-1	NPIVYGVKTK**Q**IRESVIKFLL		
*h*OR52N4	NPIVYGVKTK**Q**IRDCVIRILS		*m*OR34-5	NPVVYGVKTK**Q**IRDCVIRILS		
*h*OR52N5	NPIVYGVKTK**Q**IRKSVIKFFQ		*m*OR34-6	NPIVYGMKTK**Q**IRDSIIKFFH		
*h*OR52R1	NPIIYGVRTK**Q**IGDRVIQGCC		*m*OR30-1	NPIIYGVRTK**Q**IRDRVIRGFR		
*h*OR52W1	NPLIYGARTK**Q**IRDRLLETFT		*m*OR36-1	NPLIYGVRTK**Q**IRDRFLEMFK		
*h*OR56A3	NPIIYGVRTQ**E**IKQGMQRLLK		*m*OR40-2	NPIVYGVRTQ**E**IKQGIKKLLK		
*h*OR56A4	NPIVYGVRTK**E**IKQGIQNLLK		*m*OR40-8	NPIVYGVRTR**E**IKQGIQNLLR		
*h*OR56A5	NPIVYGVRTK**E**IKQGIQNLLR		*m*OR40-1	NPIVYGVRTR**E**IKQGIRNLLR		
*h*OR56B1	NPTVYALQTK**E**LRAAFQKVLF		*m*OR40-13	NPIVYALRTR**E**LRRGFQKVFC		
*h*OR56B4	NPLACALRMH**K**LRLGFQRLLG		*m*OR40-12	NPMVYALKNK**E**LKEGFYLCSG		

Supplementary Fig. S3. Alignment of amino acid sequences of NPxxY motif and helix 8 of olfactory receptors and non-olfactory GPCRs. The 42 pairs of human and murine class I ORs, 11 pairs of human and murine class II ORs, five pairs of human and murine TAARs, and 79 human non-olfactory GPCRs are shown. The helix-8 **2nd residue** is basically located at the 7th position from Lys of the NPxxY motif that interacts with helix-8 3rd residue in the inactive state but not in the active state. Helix 8 was expected to be formed by hydrophobic residues at the 3rd and more than two of the 7th, 8th, 10th, and 11th positions.

Human ORs			Homologous murine ORs			Subclass
mOR-S6	*TM7-NPxxY*	*helix 8*	*mOR-S6*	*TM7-NPxxY*	*helix 8*	
*h*OR1J1	NPFIYSLRNK**D**IKGALRKLLS		*m*OR136-14	NPFIYSLRNK**D**MKGALKKLLS		class II OR
*h*OR1J2	NPFIYSLRNR**D**MKEALGKLFS		*m*OR136-8	NPFIYSLRNR**D**MKGALRNMLA		
*h*OR2A1	NPLIYSLRNG**E**VKGALRRALG		*m*OR261-5	NPLIYSLRNA**E**VKGALRRSLC		
*h*OR2A2	NPLIYSLRNA**Q**LKGALHRALQ		*m*OR261-11	NPLIYSLRNT**Q**VKEAFHRALQ		
*h*OR2A4	NPLICSLRNS**E**VKNTLKRVLG		*m*OR261-6	NPLIYSLRNS**D**VKNTLKRVLR		
*h*OR2A5	NPLIYSLRNA**E**VKGALKRVLW		*m*OR261-13	NPLIYSLRNA**E**VKGAVKRVLW		
*h*OR4L1	NPSIYTLRNK**K**MQEAIRKLRF		*m*OR247-4	NPIIYTLRNQ**E**MKKAMRKLWI		
*h*OR5M8	NLIIYSLRNK**N**VKEALIKELS		*m*OR200-1	NPMIYSLRNK**D**VKEAISKELS		
*h*OR8G1	NPLIYSLRNK**D**VHVSLKKMLQ		*m*OR171-30	NPLIYSLRNK**D**VKVALTKFYE		
*h*OR9A2	NPFIFTLRND**K**VKEALRDGMK		*m*OR120-1	NPFIFTLRND**K**VKEALRDGVK		
*h*OR9A4	NPFIFTLRND**K**VIEALRDGVK		*m*OR120-2	NPFIFTLRND**K**VIEALRDGVK		
*h*TAAR1	NPMVYAFFYP**W**FRKALKMMLF		*m*TAAR1	NPMVYAFFYP**W**FRRALKMVLL		TAAR
*h*TAAR2	NPLIYGFFYP**W**FRRALKYILL		*m*TAAR2	NPLIYGFFYP**W**FRRALKYILL		
*h*TAAR5	NPIIYVFSYQ**W**FRKALKLTLS		*m*TAAR5	NPIIYVFSYR**W**FRKALKLLLS		
*h*TAAR6	NPLIYALFYP**W**FRKAIKVIVT		*m*TAAR6	NPLIYALFYP**W**FKKAIKVIMS		
*h*TAAR9	NPLIYAFFYQ**W**FGKAIKLIVS		*m*TAAR9	NPLIYAFFYP**W**FRKAIKLIVS		

Human GPCRs			Human GPCRs			Subclass.G-pr_subtypes
mOR-S6	*TM7-NPxxY*	*helix 8*	*mOR-S6*	*TM7-NPxxY*	*helix 8*	
Rhodopsin	NPVIYIMMNK**Q**FRNCMLTTIC		Opsin1SW	NPIIYCFMNK**Q**FQACIMKMVC		Rhod.G_t
Opsin1MW	NPVIYVFMNR**Q**FRNCILQLFG		Opsin1LW	NPVIYVFMNR**Q**FRNCILQLFG		Rhod.G_t
β_1 AdR	NPIIYC.RSP**D**FRKAFQGLLC		β_2 AdR	NPLIYC.RSP**D**FRIAFQELLC		AdR.G_s
β_3 AdR	NPLIYC.RSP**D**FRSAFRRLLC					Adrenergic R.G_s
α_1 AdR	NPIIYPCSSQ**E**FKKAFQNVLR					Adrenergic R.G_q
α_2 AdR	NPVIYTIFNH**D**FRRAFKKILC					Adrenergic R.G_i
D1	NPIIYAF.NA**D**FRKAFSTLLG		D5	NPVIYAF.NA**D**FQKVFAQLLG		DopR.G_s
D2	NPIIYTTFNI**E**FRKAFLKILH		D3	NPVIYTTFNI**E**FRKAFLKILS		DopR.G_i
D4	NPVIYTVFNA**E**FRNVFRKALR					Dopamine R.G_i
CT R*	VATIYCFCNN**E**VQTTVKRQWA					Calcitonin R.G_s
GHRHR*	VAILYCFLNQ**E**VRTEISRKWH		GIPR*	VSVLYCFINK**E**VQSEIRRGWH		GluR.G_s
GLP-1 R*	NPVIYTVFNA**E**FRNVFRKALR		GCGR*	VAVLYCFLNK**E**VQSELRRRWH		GluR.G_s
A_{2A}	NPFIYAYRIR**E**FRQTFRKIIR		A_{2B}	NPIVYAYRNR**D**FRYTFHKIIS		AdenR.G_s
A3	NPIVYAYKIK**K**FKETYLLILK		A1	NPIVYAFRIQ**K**FRVTFLKIWN		AdenR.G_i
5-HT_6	NPIIYPLFMR**D**FKRALGRFLP		5-HT_7	NPFIYAFFNR**D**LRTTYRSLLQ		SeroR.G_s
5-HT_4	NPFLYAFLNK**S**FRRAFLIILC					Serotonin R.G_s
5-HT_{2B}	NPLVYTLFNK**T**FRDAFGRYIT		5-HT_{2A}	NPLVYTLFNK**T**YRSAFSRYIQ		SeroR.G_q
5-HT_{2C}	NPLVYTLFNK**I**YRRAFSNYLR					Serotonin R.G_q
5-HT_{1D}	NPIIYTVFNE**E**FRQAFQKIVP		5-HT_{5A}	NPLIYTAFNK**N**YNSAFKNFFS		SeroR.G_i
5-HT_{1A}	NPVIYAYFNK**D**FQNAFKKIIK		5-HT_{1B}	NPIIYTMSNE**D**FKQAFHKLIR		SeroR.G_i
5-HT_{1E}	NPLLYTSFNE**D**FKLAFKKLIR		5-HT_{1F}	NPLIYTIFNE**D**FKKAFQKLVR		SeroR.G_i

Supplementary Fig. S3. Alignment of amino acid sequences of NPxxY motif and helix 8 of olfactory receptors and non-olfactory GPCRs (continued). The 42 pairs of human and murine class I ORs, 11 pairs of human and murine class II ORs, five pairs of human and murine TAARs, and 79 human non-olfactory GPCRs are shown. The helix-8 **2nd residue** is basically located at the 7th position from Lys of the NPxxY motif that interacts with helix-8 3rd residue in the inactive state but not in the active state. Helix 8 was expected to be formed by hydrophobic residues at the 3rd and more than two of the 7th, 8th, 10th, and 11th positions.

	Human GPCRs		Human GPCRs	Subclass.G-pr_subtypes
mOR-S6	*TM7-NPxxY* *helix 8*	*mOR-S6*	*TM7-NPxxY* *helix 8*	
H2	NPILYAALNR**D**FRTGYQQLFC			Histamine R.G_q>G_s
H1	NPLIYPLCNE**N**FKKTFKRILH			Histamine R.G_q
H4	NPLLYPLCHK**R**FQKAFLKIFC	H3	NPVLYPLCHH**S**FRRAFTKLLC	HistR.G_i
MC1	DPLIYAFHSQ**E**LRRTLKEVLT	MC2	DPFIYAFRSP**E**LRDAFKKMIF	MelaR.G_s
MC3	DPLIYAFRSL**E**LRNTFREILC	MC4	DPLIYALRSQ**E**LRKTFKEIIC	MelaR.G_s
MC5	DPLIYAFRSQ**E**MRKTFKEIIC			Melanocortin R.G_s
V2	NPWIYASFSS**S**VSSELRSLLC			Vasopressin R.G_s
V1a	NPWIYMFFSG**H**LLQDCVQSFP	V1b	NPWIYMGFNS**H**LLPRPLRHLA	VassR.G_q
OXTR	NPWIYMLFTG**H**LFHELVQRFL			Oxytocin R.G_q
SSTR3	NPILYGFLSY**R**FKQGFRRVLL			Somatstatin R.G_i>G_q
SSTR1	NPILYGFLSD**N**FKRSFQRILC	SSTR2	NPILYAFLSD**N**FKKSFQNVLC	SomaR.G_i
SSTR4	NPILYGFLSD**N**FRRFFQRVLC	SSTR5	NPVLYGFLSD**N**FRQSFQKVLC	SomaR.G_i
FSH	NPFLYAIFTK**N**FRRDFFILLS			Glycoprotein hormone R.G_s/G_i/G_q
LH	NPFLYAIFTK**T**FQRDFFLLLS	TSH	NPFLYAIFTK**A**FQRDVFILLS	GlyHR.G_s>G_q
δOpioid	NPVLYAFLDE**N**FKRCFRQLCR	κOpioid	NPILYAFLDE**N**FKRCFRDFCF	OpioR.G_i
μOpioid	NPVLYAFLDE**N**FKRCFREFCI	ORL1	NPILYAFLDE**N**FKACFRKFCC	OpioR.G_i
XCR1	NPVLYVFVGV**K**FRTHLKHVLR			Chemokine(C) R.G_i
CCR2	NPIIYAFVGE**K**FRSLFHIALG	CCR4	NPIIYFFLGE**K**FRKYILQLFK	ChemR.G_i
CCR5	NPIIYAFVGE**K**FRNYLLVFFQ	CCR6	NPVLYAFIGQ**K**FRNYFLKILK	ChemR.G_i
CCR7	NPFLYAFIGV**K**FRNDLFKLFK	CCR8	NPVIYAFVGE**K**FKKHLSEIFQ	ChemR.G_i
CCR1	NPVIYAFVGE**R**FRKYLRQLFH	CCR3	NPVIYAFVGE**R**FRKYLRHFFH	ChemR.G_i
CCR9	NPVLYVFVGE**R**FRRDLVKTLK	CCR10	NPVLYAFLGL**R**FRQDLRRLLR	ChemR.G_i
CXCR2	NPLIYAFIGQ**K**FRHGLLKILA	CXCR3	NPLLYAFVGV**K**FRERMWMLLL	ChemR.G_i
CXCR6	NPVLYAFVSL**K**FRKNFWKLVK	CXCR5	NPMLYTFAGV**K**FRSDLSRLLT	ChemR.G_i
CXCR4	NPILYAFLGA**K**FKTSAQHALT			Chemokine(CXC) R.G_i
CXCR1	NPIIYAFIGQ**N**FRHGFLKILA	CXCR7	NPVLYSFINR**N**YRYELMKAFI	ChemR.G_i
CX3CR1	NPLIYAFAGE**K**FRRYLYHLYG			Chemokine(CX3C) R.G_i

Supplementary Fig. S3. Alignment of amino acid sequences of NPxxY motif and helix 8 of olfactory receptors and non-olfactory GPCRs (continued). The 42 pairs of human and murine class I ORs, 11 pairs of human and murine class II ORs, five pairs of human and murine TAARs, and 79 human non-olfactory GPCRs are shown. The helix-8 **2nd residue** is basically located at the 7th position from Lys of the NPxxY motif that interacts with helix-8 3rd residue in the inactive state but not in the active state. Helix 8 was expected to be formed by hydrophobic residues at the 3rd and more than two of the 7th, 8th, 10th, and 11th positions. Calcitonin receptor (CT R*), growth hormone releasing hormone receptor (GHRHR*), gastric inhibitory polypeptide receptor (GIPR*), glucagon-like peptide-1 receptor (GLP-1 R*) and glucagon receptor (GCGR*) belong to the class B family of GPCRs, some of which conserve TM7 V(A/S)(V/I/T)(L/I)Y and helix-8 V8.50 instead of the NPxxY motif and F8.50 [37].

Supplementary Table ST1. Classification of olfactory receptors and other GPCRs by helix 8-2nd residues and subtypes of G proteins.

GPCRs	Helix-8 Second Residue										Predicted Hierarchy or the 2nd residue
	all	Glu	Gln	Asp	Asn	Trp	His	Lys	Arg	misc	
Angiotensin II R 1 (hormone, $G_{i/o}$, $G_{q/11}$)	1 100%	0 0%	0 0%	0 0%	0 0%	0 0%	0 0%	**1 100%**	0 0%	0 0%	R1(K) > R2(R)/L1(R) (G_i) ?
Angiotensin II 2/L1 Rs (hormone, $G_{i/o}$)	2 100%	0 0%	0 0%	0 0%	0 0%	0 0%	0 0%	0 0%	**2 100%**	0 0%	
Bradykinin 2 R (peptide chemokine, G_s, $G_{i/o}$, $G_{q/11}$)	1 100%	0 0%	0 0%	0 0%	0 0%	0 0%	0 0%	0 0%	**1 100%**	0 0%	R2(R) > R1(L) (G_i)
Bradykinin 1 R (peptide chemokine, $G_{i/o}$, $G_{q/11}$)	1 100%	0 0%	0 0%	0 0%	0 0%	0 0%	0 0%	0 0%	0 0%	**1 100%**	R1(L)
Neuropeptides B/W1/2 Rs (neuropeptide, $G_{i/o}$)	2 100%	0 0%	0 0%	0 0%	1 50%	0 0%	0 0%	0 0%	0 0%	1 50%	R2(N) > R1(S) (G_i)
Neuropeptides FF1/2 Rs (neuropeptide, $G_{i/o}$)	2 100%	0 0%	0 0%	0 0%	**2 100%**	0 0%	0 0%	0 0%	0 0%	0 0%	
Galanin 2 R (neuropeptide, $G_{q/11}$)	1 100%	0 0%	0 0%	0 0%	0 0%	0 0%	**1 100%**	0 0%	0 0%	0 0%	
Galanin 1/3 Rs (neuropeptide, $G_{i/o}$)	2 100%	0 0%	0 0%	0 0%	1 50%	0 0%	1 50%	0 0%	0 0%	0 0%	R3(H) > R1(N) (G_i)
Cysteinyl leukotriene 1/2 Rs (eicosanoid, $G_{q/11}$)	2 100%	0 0%	0 0%	0 0%	**2 100%**	0 0%	0 0%	0 0%	0 0%	0 0%	
Leukotriene B4 R2 (eicosanoids, $G_{i/o}$)	1 100%	0 0%	0 0%	**1 100%**	0 0%	0 0%	0 0%	0 0%	0 0%	0 0%	R2(D) > R(G) (G_i)
Leukotriene B4 R (eicosanoids, $G_{i/o}$, $G_{q/11}$)	1 100%	0 0%	0 0%	0 0%	0 0%	0 0%	0 0%	0 0%	0 0%	**1 100%**	R(G)
Oxoeicosanoid R (eicosanoids, $G_{i/o}$, $G_{q/11}$)	1 100%	0 0%	0 0%	**1 100%**	0 0%	0 0%	0 0%	0 0%	0 0%	0 0%	
Rexaxin/insulin-like family peptide 1/2 Rs (peptide hormones, G_s, $G_{i/o}$)	2 100%	0 0%	0 0%	0 0%	0 0%	0 0%	0 0%	0 0%	0 0%	2 100%	R1(P) > R2(F) (G_s)
Rexaxin/insulin-like family peptide 3/4 Rs (peptide hormones, $G_{i/o}$)	2 100%	**2 100%**	0 0%	0 0%	0 0%	0 0%	0 0%	0 0%	0 0%	0 0%	
Cholecystokinin A/B Rs (peptide hormones, $G_{q/11}$)	2 100%	0 0%	0 0%	0 0%	0 0%	0 0%	0 0%	0 0%	**2 100%**	0 0%	
Hypocretin (orexin) 1/2 Rs (peptide hormones, G_s, $G_{i/o}$, $G_{q/11}$)	2 100%	0 0%	0 0%	0 0%	0 0%	0 0%	0 0%	**2 100%**	0 0%	0 0%	
BRS3, NMBR, GRPR (peptide, $G_{q/11}$)	3 100%	0 0%	0 0%	0 0%	0 0%	0 0%	0 0%	0 0%	0 0%	**3 100%**	(S, S, S)
Endothelin A/B Rs (peptide, G_s, $G_{q/11}$)	2 100%	0 0%	0 0%	0 0%	0 0%	0 0%	0 0%	1 50%	1 50%	0 0%	A(K) > B(R) (G_q)?
Neuromedin U 1/2 Rs (peptide, $G_{q/11}$)	2 100%	0 0%	0 0%	0 0%	0 0%	0 0%	0 0%	0 0%	**2 100%**	0 0%	
Neurotensin 1/2 Rs (peptide, $G_{q/11}$)	2 100%	0 0%	0 0%	0 0%	1 50%	0 0%	0 0%	0 0%	0 0%	1 50%	R1(N) > R2(S) (G_q)
Anaphylatoxin C3A/C5A/CMKL1 Rs (peptide, $G_{i/o}$?)	3 100%	0 0%	0 0%	2 67%	0 0%	0 0%	0 0%	0 0%	0 0%	1 33%	C3A(D)/CMKL(D) > C5A(G)
Formyl peptide L2 R (peptide, $G_{i/o}$, $G_{q/11}$)	1 100%	0 0%	0 0%	0 0%	**1 100%**	0 0%	0 0%	0 0%	0 0%	0 0%	L2(N) > 1(D)/L1(D) (G_i)
Formyl peptide 1/L1 Rs (peptide, $G_{i/o}$)	2 100%	0 0%	0 0%	**2 100%**	0 0%	0 0%	0 0%	0 0%	0 0%	0 0%	
Melatonin 1A/B Rs (hormone, $G_{i/o}$)	2 100%	0 0%	0 0%	0 0%	**2 100%**	0 0%	0 0%	0 0%	0 0%	0 0%	NAxxY motif mutant
Tachykinin 1/2 Rs (peptide, G_s, $G_{q/11}$)	2 100%	0 0%	0 0%	0 0%	0 0%	0 0%	0 0%	0 0%	**2 100%**	0 0%	
Tachykinin 3 R (peptide, $G_{q/11}$)	1 100%	0 0%	0 0%	0 0%	0 0%	0 0%	0 0%	0 0%	**1 100%**	0 0%	
Neuropeptides Y 2/4 Rs (neuropeptide, $G_{i/o}$, $G_{q/11}$)	2 100%	0 0%	0 0%	0 0%	**2 100%**	0 0%	0 0%	0 0%	0 0%	0 0%	R1(N)/2(N)/4(N) > R5(G) (G_i)
Neuropeptides Y 1/5 Rs (neuropeptide, $G_{i/o}$)	2 100%	0 0%	0 0%	0 0%	1 50%	0 0%	0 0%	0 0%	0 0%	1 50%	R1(N) > R5(G) (G_i)
Neuropeptides S R (neuropeptide, $G_{q/11}$, G_s)	1 100%	0 0%	0 0%	0 0%	0 0%	0 0%	0 0%	0 0%	0 0%	**1 100%**	NPSR(S)
Free fatty acid 1/2/4 Rs (lipid, $G_{q/11}$)	3 100%	1 33%	0 0%	0 0%	0 0%	0 0%	0 0%	0 0%	1 33%	1 33%	R1(G)/2(V)/4(E)
Free fatty acid 3 R (lipid, $G_{i/o}$)	1 100%	0 0%	0 0%	0 0%	0 0%	0 0%	0 0%	0 0%	0 0%	**1 100%**	R3(G)

Subtypes of target G proteins were obtained from http://www.guidetopharmacology.org. BRS3, bombesin receptor subtype 3; NMBR, neuromedin B receptor; GRPR, gastrin releasing peptide receptor; C3AR1, complement C3a receptor 1; C5AR1, complement C5a receptor 1; CMKLR1, chemerin chemokine-like receptor 1.

Supplementary Table ST1. Classification of olfactory receptors and other GPCRs by helix 8-2nd residues and subtypes of G proteins (continued).

GPCRs	Helix-8 Second Residue										Predicted Hierarchy or the 2nd residue
	all	Glu	Gln	Asp	Asn	Trp	His	Lys	Arg	misc	
Purinergic P2Y11 R (nucleotide, $G_{q/11} > G_s$)	1 100%	0 0%	0 0%	0 0%	0 0%	0 0%	0 0%	0 0%	0 0%	**1** **100%**	R11(S)
Purinergic P2Y8/10 Rs (nucleotide, ?)	2 100%	**2** **100%**	0 0%	0 0%	0 0%	0 0%	0 0%	0 0%	0 0%	0 0%	
Purinergic P2Y1 R (nucleotide, $G_{q/11} > G_{i/o}$)	1 100%	0 0%	0 0%	0 0%	0 0%	0 0%	0 0%	0 0%	0 0%	**1** **100%**	R1(T)
Purinergic P2Y2 R (nucleotide, $G_{q/11} > G_{i/o}/G_{12}$)	1 100%	0 0%	0 0%	0 0%	0 0%	0 0%	0 0%	0 0%	**1** **100%**	0 0%	
Purinergic P2Y4 R (nucleotide, $G_{q/11}$)	1 100%	0 0%	0 0%	0 0%	0 0%	0 0%	0 0%	**1** **100%**	0 0%	0 0%	
Purinergic P2Y6 R (nucleotide, $G_{q/11} > G_{12}$)	1 100%	0 0%	0 0%	0 0%	0 0%	0 0%	0 0%	**1** **100%**	0 0%	0 0%	
Purinergic P2Y12/13/14 Rs (nucleotide, $G_{i/o}$)	3 100%	0 0%	0 0%	0 0%	0 0%	0 0%	0 0%	1 33%	0 0%	2 67%	R13(K) > R14(P), R12(S)
Cannabinoid 1/2 Rs (neuropeptide, $G_{i/o}$)	2 100%	1 50%	0 0%	1 50%	0 0%	0 0%	0 0%	0 0%	0 0%	0 0%	R1(D) > R2(E) (G_i) R2(E) > R1(D) (G_s)
GPER1 (GPR30) (hormone, G_s, $G_{i/o}$, $G_{q/11}$)	1 100%	0 0%	0 0%	0 0%	0 0%	0 0%	0 0%	0 0%	0 0%	**1** **100%**	R1(T)
LPAR1/2 (lipid signal, $G_{i/o}$, $G_{q/11}$, G_{12})	2 100%	**2** **100%**	0 0%	0 0%	0 0%	0 0%	0 0%	0 0%	0 0%	0 0%	
LPAR3 (lipid signal, $G_{i/o}$, $G_{q/11}$)	1 100%	0 0%	0 0%	**1** **100%**	0 0%	0 0%	0 0%	0 0%	0 0%	0 0%	
LPAR4 (lipid signal, G_s, $G_{i/o}$, $G_{q/11}$, G_{12})	1 100%	0 0%	0 0%	0 0%	0 0%	0 0%	0 0%	0 0%	0 0%	**1** **100%**	R4(S)
LPAR6 (lipid signal, G_s, $G_{i/o}$, G_{12})	1 100%	0 0%	0 0%	0 0%	0 0%	0 0%	0 0%	0 0%	0 0%	**1** **100%**	R6(T)
LPAR5 (lipid signal, $G_{q/11}$, G_{12})	1 100%	0 0%	0 0%	0 0%	0 0%	0 0%	0 0%	0 0%	0 0%	**1** **100%**	R5(G)
S1PR1 (lipid mediator, $G_{i/o}$)	1 100%	**1** **100%**	0 0%	0 0%	0 0%	0 0%	0 0%	0 0%	0 0%	0 0%	
S1PR3 (lipid mediator, $G_{i/o}$, $G_{q/11}$, $G_{12/13}$)	1 100%	**1** **100%**	0 0%	0 0%	0 0%	0 0%	0 0%	0 0%	0 0%	0 0%	
S1PR4/5 (lipid mediator, $G_{i/o}$, $G_{12/13}$)	2 100%	1 50%	0 0%	1 50%	0 0%	0 0%	0 0%	0 0%	0 0%	0 0%	R4(E) = R5(D) (G_i)
S1PR2 (lipid mediator, G_s, $G_{q/11}$, $G_{12/13}$)	1 100%	0 0%	0 0%	**1** **100%**	0 0%	0 0%	0 0%	0 0%	0 0%	0 0%	
Prostanoid PTGD/PTGE2 Rs (eicosanoids, G_s)	2 100%	0 0%	0 0%	0 0%	0 0%	0 0%	0 0%	0 0%	0 0%	**2** **100%**	D(P)/E2(P)
Prostanoid PTGE4/PTGI Rs (eicosanoids, $G_s > G_{i/o}$)	2 100%	0 0%	0 0%	0 0%	1 50%	0 0%	0 0%	0 0%	0 0%	1 50%	E4(T) > I(A) (G_s)
Prostanoid PTGE1/PTGF/TBXA2 Rs (eicosanoids, $G_{q/11}$)	3 100%	0 0%	0 0%	0 0%	0 0%	0 0%	0 0%	0 0%	0 0%	**3** **100%**	E1(A)/F(A), TBXA2(A)
Prostanoid PTGE3/PTGD2 Rs (eicosanoids, $G_{i/o}$)	2 100%	0 0%	0 0%	1 50%	0 0%	0 0%	0 0%	0 0%	0 0%	1 50%	E3(I) > D2(D) (G_i)
Orphan GPR4 R (?, G_s, $G_{i/o}$ $G_{q/11}$, $G_{12/13}$)	1 100%	0 0%	0 0%	0 0%	0 0%	0 0%	0 0%	0 0%	0 0%	**1** **100%**	R4(G)
Orphan GPR65 R (?, G_s)	1 100%	0 0%	0 0%	0 0%	0 0%	0 0%	0 0%	0 0%	0 0%	**1** **100%**	R65(T)
Orphan GPR18/68 Rs (?, $G_{i/o}$, $G_{q/11}$)	2 100%	0 0%	1 50%	0 0%	0 0%	0 0%	0 0%	0 0%	0 0%	1 50%	R18(Q) > R68(T)
Orphan GPR17/20/35 Rs (?, $G_{i/o}$)	3 100%	1 33%	0 0%	0 0%	0 0%	0 0%	0 0%	1 33%	0 0%	1 33%	R17(K) > R35(E)/20(G) (G_i)
Orphan GPR55 R (?, $G_{q/11}$, $G_{12/13}$)	1 100%	**1** **100%**	0 0%	0 0%	0 0%	0 0%	0 0%	0 0%	0 0%	0 0%	
MAS1/MAS1L oncogene (?, $G_{i/o}$, $G_{q/11}$)	2 100%	0 0%	0 0%	0 0%	0 0%	0 0%	0 0%	0 0%	0 0%	2 100%	no helix 8 (S or R, L or R)
ADGRB1/2/3* (secretin, $G_{i/o}$?)	3 100%	**3** **100%**	0 0%	0 0%	0 0%	0 0%	0 0%	0 0%	0 0%	0 0%	

Subtypes of target G proteins were obtained from http://www.guidetopharmacology.org. Brain-specific angiogenesis inhibitors (ADGRB1/2/3*) belong to the class B* family of GPCRs and uniquely conserve TM7 FVI(V/T)(M/A)VH motif and helix-8 V8.50 instead of the NPxxY motif and F8.50. GPER1, G protein-coupled estrogen receptor 1; LPAR, lysophosphatidic acid receptor; PTGDR, prostaglandin D2 receptor; PTGER1/2/3/4, prostaglandin E receptor 1/2/3/4; PTGFR, prostaglandin F receptor; PTGIR, prostaglandin I2 receptor; TBXA2R, thromboxane A2 receptor; MAS1, MAS1 proto-oncogene G protein-coupled receptor; MAS1L, MAS1 proto-oncogene like, G protein-coupled receptor.

Human GPCRs			Human GPCRs			Subclass.G-pr_subtypes
mOR-S6	*NPxxY*	*helix 8*	*mOR-S6*	*NPxxY*	*helix 8*	
AGT1R	NPLFYGFLGK**K**FKRYFLQLLK					Angiotensin II R.G_q/G_i/G_{12}
AGT2R	NPFLYCFVGN**R**FQQKLRSVFR		AGTRL1	NPFLYAFFDP**R**FRQACTSMLC		AngIIR.$G_{i/o}$
BDKRB2	NPLVYVIVGK**R**FRKKSWEVYQ					Bradykinin R.G_s/G_i/G_q
BDKRB1	NPVIYVFVGR**L**FRTKVWELYK					Bradykinin R.G_i/G_q
NPBWR2	NPFLYAFLDD**N**FRKNFRSILR		NPBWR1	NPFLYAFLDA**S**FRRNLRQLIT		NeurPB.G_i
NPFFR1	NPIIYGYFNE**N**FRRGFQAAFR		NPFFR2	NPIIYGFFNE**N**FRRGFQEAFQ		NeurPF.G_i
GALR2	NPIVYALVSK**H**FRKGFRTICA					Galanin R.G_q
GALR3	NPLVYALASR**H**FRARFRRLWP		GALR1	NPIIYAFLSE**N**FRKAYKQVFK		GalR.G_i
CYSLTR1	DPLLYFFSGG**N**FRKRLSTFRK		CYSLTR2	NPLLYYFAGE**N**FKDRLKSALR		CysLeR.G_q>G_i
LTB4R2	NPVLYVFTAG**D**LLPRAGPRFL					Leukotriene B4 R.$G_{i/o}$>G_q
LTB4R	NPVLYACAGG**G**LLRSAGVGFV					Leukotriene B4 R.G_i/G_q
OXER	DPVLYCFSSP**N**FLHQSRALLG					Oxoeicosanoid R.G_i
RXFP1	NPILYTLTTR**P**FKEMIHRFWY		RXFP2	NPILYTLTTN**F**FKDKLKQLLH		RelaxR.G_s/G_i
RXFP3	NPVLYCLVRR**E**FRKALKSLLW		RXFP4	NPVLYCLLRR**E**PRQALAGTFR		RelaxR.G_i
CCKAR	NPIIYCFMNK**R**FRLGFMATFP		CCKBR	NPLVYCFMHR**R**FRQACLETCA		CholeR.G_q
HCRTR1	NPIIYNFLSG**K**FREQFKAAFS		HCRTR2	NPIIYNFLSG**K**FREEFKAAFS		OrexnR.G_s/G_i/G_q
BRS3	NPFALYWLSK**S**FQKHFKAQLF		NMBR	NPFALYLLSE**S**FRRHFNSQLC		BombR.G_q
GRPR	NPFALYLLSK**S**FRKQFNTQLL					Gastrin releasing peptide R.G_q
EDNRA	NPIALYFVSK**K**FKNCFQSCLC					Endthelin R.G_q
EDNRB	NPIALYLVSK**R**FKNCFKSCLC					Endthelin R.G_s/G_i/G_q
NMUR1	NPVLYSLMSS**R**FRETFQEALC		NMUR2	NPIIYNLLSR**R**FQAAFQNVIS		NeurMR.G_q
NTSR1	NPILYNLVSA**N**FRHIFLATLA		NTSR2	TPLLYNAVSS**S**FRKLFLEAVS		NeurTR.G_q
C3AR1	NPFLYALLGK**D**FRKKARQSIQ		C5AR1	NPIIYVVAGQ**G**FQGRLRKSLP		AnaphR.$G_{i?}$
CMKLR1	NPILYVFMGQ**D**FKKFKVALFS					Chemokine-like R1(Anaphylatoxin R).G_i
FPR3	NPILYVFMGR**N**FQERLIRSLP					Formyl peptide R.G_i>G_q
FPR1	NPMLYVFMGQ**D**FRERLIHALP		FPR2	NPMLYVFVGQ**D**FRERLIHSLP		FormP.G_i
MTNR1A	NAIIYGLLNQ**N**FRKEYRRIIV		MTNR1B	NAIVYGLLNQ**N**FRREYKRILL		MelanR.G_i
TACR1	NPIIYCCLND**R**FRLGFKHAFR		TACR2	NPIIYCCLNH**R**FRSGFRLAFR		TachyR.G_s/G_q
TACR3	NPIIYCCLNK**R**FRAGFKRAFR					Tachykinin R.G_q
NPY2R	NPLLYGWMNS**N**YRKAFLSAFR		NPY4R	NPFIYGFLNT**N**FKKEIKALVL		NePYR.G_i>G_q
NPY1R	NPIFYGFLNK**N**FQRDLQFFFN		NPY5R	NPILYGFLNN**G**IKADLVSLIH		NePYR.G_i
NPSR	NPLIYCVFSSSI**S**FPCRVIRL					Neuropeptides S R.G_q/G_s
FFAR1	NPLVTGYLGR**G**PGLKTVCAAR		FFAR2	DPLLFYFSSS**V**VRRAFGRGLQ		FreeFAR.G_q
FFAR4	NPILYNMTLCRN**E**WKKIFCCF					Free fatty acid R.G_q
FFAR3	DPFVYYFSSS**G**FQADFHELLR					Free fatty acid R.G_i

Supplementary Fig. S4. Alignment of amino acid sequences of NPxxY motif and helix 8 of GPCRs. The 99 human GPCRs and target G proteins (from http://www.guidetopharmacology.org) are shown. The helix-8 **2nd residue** is basically located at the 7th position from Lys of the NPxxY motif that interacts with helix-8 3rd residue in the inactive state but not in the active state. Helix 8 was expected to be formed by hydrophobic residues at the 3rd and more than two of the 7th, 8th, 10th, and 11th positions. Some of their helical structures are likely to be unstable. NPSR and FFAR4 may cause a shift in the position of helix 8 by two amino acids. BRS3, bombesin receptor subtype 3; NMBR, neuromedin B receptor; ENDRA/B, endotheline receptor type A/B; NMUR, neuromedin U receptor; NTSR, neurotensin receptor; C3AR1, complement C3a receptor 1; C5AR1, complement C5a receptor 1; CMKLR1, chemerin chemokine-like receptor 1; FPR, formyl peptide receptor; MTNR1A/B, melatonin receptor 1A/B; NPY1/2/4/5R, neuropeptide Y receptor Y1/2/4/5.

	Human GPCRs			Human GPCRs	Subclass.G-pr_subtypes
mOR-S6	*NPxxY*	*helix 8*	*mOR-S6*	*NPxxY*	*helix 8*	
P2RY1	DPILYFLAGD**T**FRRRLSRATR				Purinergic P2Y R.G_q>G_i
P2RY2	DPVLYFLAGQ**R**LVRFARDAKP				Purinergic P2Y R.G_q>G_i/G_{12}
P2RY4	DPVLYLLTGD**K**YRRQLRQLCG				Purinergic P2Y R.G_q
P2RY6	DPILFYFTQK**K**FRRRPHELLQ				Purinergic P2Y R.G_q>G_s
P2RY8	DPFVYYFASR**E**FQLRLREYLG	P2RY10	DPILYYFMAS**E**FRDQLSRHGS		P2Y R.?
P2RY11	HPLLYMAAVP**S**LGCCCRHCPG				Purinergic P2Y R.G_q>G_s
P2RY12	DPFIYFFLCK**S**FRNSLISMLK	P2RY13	DPLIYIFLCK**K**FTEKLPCMQG		P2Y R.G_i
P2RY14	DPIIYFFLCQ**P**FREILCKKLH				Purinergic P2Y P2Y R.G_i
CNR1	NPIIYALRSK**D**LRHAFRSMFP	CNR2	NPVIYALRSG**E**IRSSAHHCLA		CannR.G_i>G_s
GPER1	NPLIYSFLGE**T**FRDKLRLYIE				GP Estrogen R1.G_s
LPAR1	NPIIYSYRDK**E**MSATFRQILC	LPAR2	NAAVYSCRDA**E**MRRTFRRLLC		LisAR.G_i/G_q/G_{12}
LPAR3	NPIIYSYKDE**D**MYGTMKKMIC				Lisophosphatidic acid R.G_i/G_q
LPAR4	DPFIYYFTLE**S**FQKSFYINAH				Lisophosphatidic acid R.G_s/G_i/G_q/G_{12}
LPAR6	DPIVYYFTSD**T**IQNSIKMKNW				Lisophosphatidic acid R.G_s/G_i/G_{12}
LPAR5	DPLVYYFSAE**G**FRNTLRGLGT				Lisophosphatidic acid R.G_q/G_{12}
S1PR1	NPIIYTLTNK**E**MRRAFIRIMS				Sphingosine-1-phosphate R.G_i
S1PR2	NPVIYTWRSR**D**LRREVLRPLQ				Sphingosine-1-phosphate R.G_s/G_q/G_{12}
S1PR3	NPVIYTLASK**E**MRRAFFRLVC				Sphingosine-1-phosphate R.G_i/G_q/G_{12}
S1PR4	NPIIYSFRSR**E**VCRAVLSFLC	S1PR5	NPIIYTLTNR**D**LRHALLRLVC		SphPR.G_i/G_{12}
PTGDR	DPWIFIIFRS**P**VFRIFFHKIF	PTGER2	DPWVFAILRP**P**VLRLMRSVLC		ProsR.G_s
PTGER4	DPWIYILLRK**T**VLSKAIEKIK				Prostagrandin R.G_s>G_i
PTGIR	DPWVFILFRK**A**VFQRLKLWVC				Prostagrandin R.G_s>G_i/G_q
PTGER1	DPWVYILLRQ**A**VLRQLLRLLP				Prostagrandin R.G_q>G_i
PTGFR	DPWVYILLRK**A**VLKNLYKLAS				Prostagrandin R.G_q>G_s
TBXA2R	DPWVYILFRR**A**VLRRLQPRLS				Prostagrandin R.G_q
PTGER3	DPWVYLLLRK**I**LLRKFCQIRY				Prostagrandin R.G_i>G_q
PTGDR2	NPVLYVLTCP**D**MLRKLRRSLR				Prostagrandin R.G_i
GPR4	DPILYCLVNE**G**ARSDVAKALH				orphan clsA15.G_s/G_i/G_q/G_{12}
GPR65	DPILYCFVTE**T**GRYDMWNILK				orphan clsA15.G_s
GPR18	DVILYYIVSK**Q**FQARVISVML	GPR68	DPVLYCFVSE**T**THRDLARLRG		clsA15.G_i/G_q
GPR17	DPIMYFFVAE**K**FRHALCNLLC				orphan clsA15.G_i>G_q
GPR20	DPIVYCFVTS**G**FQATVRGLFG	GPR35	DAICYYYMAK**E**FQEASALAVA		clsA15.G_i
GPR55	DVFCYYFVIK**E**FRMNIRAHRP				orphan clsA15.G_q/G_{12}
MAS1	NPFIYFFVGSSKKK**R**FKESLK	MAS1L	NPIIYFFVGSLRKK**R**LKESLR		MAS1R.G_i/G_q
ADGRB1*	FVIVMVHCILRR**E**VQDAVKCRVV	ADGRB2*	FVITAVHCFLRR**E**VQDVVKCQMG		BraAR.G_i?
ADGRB3*	FVIVMVHCILRR**E**VQDAFRCRLR	Brain-specific angiogenesis inhibitor.G_i?			

Supplementary Fig. S4. Alignment of amino acid sequences of NPxxY motif and helix 8 of non-olfactory GPCRs (continued). The 99 human GPCRs and target G proteins (from http://www.guidetopharmacology. org) are shown. The helix-8 **2nd residue** is basically located at the 7th position from Lys of the NPxxY motif that interacts with helix-8 3rd residue in the inactive state but not in the active state. Helix 8 was expected to be formed by hydrophobic residues at the 3rd and more than two of the 7th, 8th, 10th, and 11th positions. Brain-specific angiogenesis inhibitors (ADGRB1*, ADGRB2*, ADGRB3*: class B) uniquely conserve TM7 FVI(V/T)(M/A)VH motif and helix-8 V8.50 instead of the NPxxY motif and F8.50. Some of their helical structures are likely to be unstable. CNR, cannabinoid receptor; GPER1, G protein-coupled estrogen receptor 1; PTGDR, prostaglandin D2 receptor; PTGER1/2/3/4, prostaglandin E receptor 1/2/3/4; PTGFR, prostaglandin F receptor; PTGIR, prostaglandin I2 receptor; TBXA2R, thromboxane A2 receptor; MAS1, MAS1 proto-oncogene G protein-coupled receptor; MAS1L, MAS1 proto-oncogene like, G protein-coupled receptor.